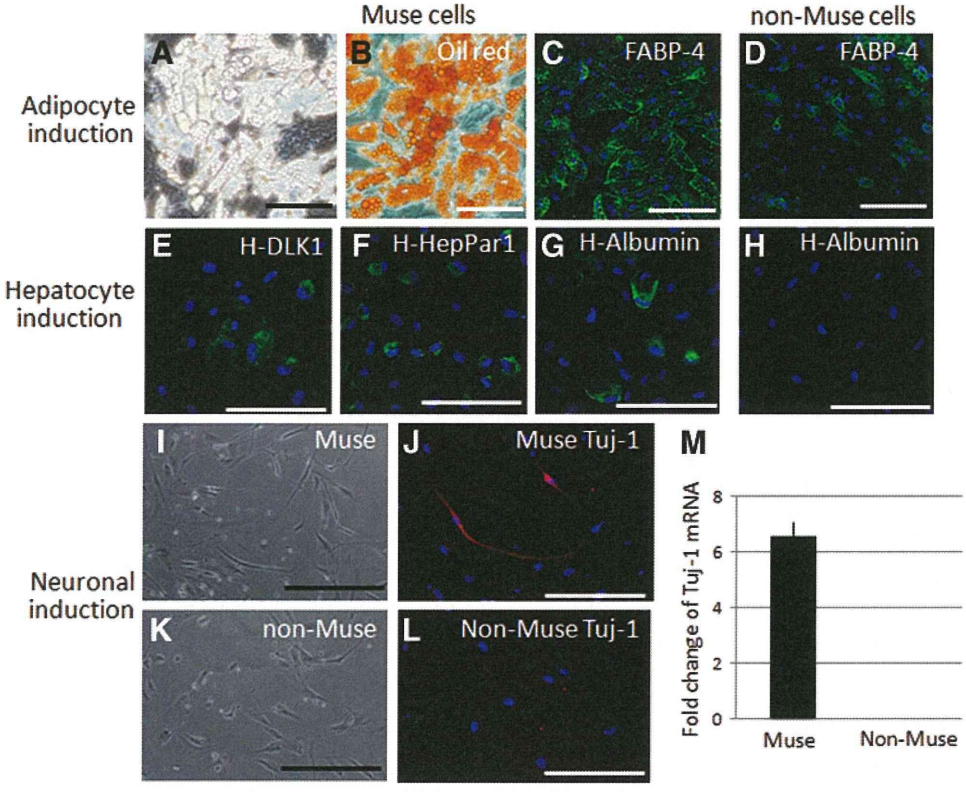

FIG. 6. Induced differentiation of adipose-Muse and -non-Muse cells. **(A–D)** Muse **(A–C)** and non-Muse **(D)** cells from LA-MSCs were subjected to adipocyte induction. Cells with lipid droplets **(A)** that are stained with Oil Red-O **(B)** were detected in adipose-Muse cells. Those cells were also positive for the adipocyte marker FABP-4. Adipose-non-Muse cells also contained cells positive for FABP-4 but with lower ratio **(D). (E–H)** After hepatocyte induction, Muse cells were positive for liver stem cell marker human-DLK1 **(E)** and hepatocyte markers human HepPar1 **(F)** and human albumin **(G)**, while non-Muse cells lacked these expression. An example of non-Muse cells was shown in human albumin expression **(H). (I–M)** After neuronal induction, Muse cells demonstrated a morphology similar to neuronal cells **(I)**, and some were also positive for Tuj-1 **(J)**. However, adipose-non-Muse cells were not like neuronal cells **(K)** and all cells were Tuj-1 negative **(L)**. Q-PCR consistently detected *Tuj-1* signal only in Muse cells and not in non-Muse cells **(M)**. Scale bars = 100 μm. Color images available online at www.liebertpub.com/scd

and LA-MSCs (adipose-Muse) were subjected to next generation sequencing to compare expression levels of genes related to endodermal, mesodermal, and ectodermal differentiation (Table 1). Analysis of mesodermal lineage expression revealed that osteogenic, adipogenic, and myogenic genes were generally higher in adipose-Muse rather than BM-Muse or dermal-Muse cells, and some of the factors, such as SP7, osteogenic factor, and Pax7 muscle stem cell marker, were only detected in adipose-Muse cells. Different from mesodermal factors, endodermal factors were more predominantly expressed in BM-Muse cells than in adipose-Muse cells. However, cholesterol 7, alpha-hydroxylase (CYP7A1), insulin gene enhancer binding protein (ISL1), and hepatocyte nuclear factor 4 alpha (HNF4A) were only expressed in adipose-Muse cells and not in BM-Muse or dermal-Muse cells (Table 1). Ectodermal genes that relate to neuronal differentiation were higher in both BM-Muse and dermal-Muse cells than in adipose-Muse cells while factors such as genes encoding for musashi RNA-binding protein 1 (MSI1), ISL1, and myelin transcription factor 1-like (MYT1L) were not expressed in BM-Muse or dermal-Muse cells, but only in adipose-Muse cells (Table 1).

Discussion

In this study, we demonstrate that both adult human subcutaneous adipose tissue and commercially available adipose-MSCs contain a small percentage of stem cells with the capacity for triploblastic differentiation and self-renewal. These cells do not undergo tumorigenic proliferation in vitro, nor do they elicit teratomas when transplanted in vivo. These characteristics match those of previously reported Muse cells that were isolated from the BM and dermis [16,17,21], indicating that adipose tissue also contains Muse cells.

In adipose tissue, single-cell-derived cluster formation in suspension was unique to adipose-Muse cells; however, cluster formation ratio did not always reach 100% (Supplementary Table S1). This may be in part because of cellular damage caused by laser irradiation in the process of FACS isolation. Alternatively, cells might have been in an inactive dormant state, such that they did not proliferate. This property of Muse cells requires further study.

While MSCs are known to provide trophic and anti-inflammatory effects, these effects are temporary and do not

TABLE 1. COMPARISON OF GENE EXPRESSION RELATED TO THE DIFFERENTIATION OF ENDODERMAL, MESODERMAL, AND ECTODERMAL LINEAGES AMONG ADIPOSE-MUSE CELLS VERSUS DERMAL- AND BM-MUSE CELLS

Mesodermal		
	Adipose / Dermal	Adipose / BM
PPARG	1.8939	3.0752
CEBPA	1.6335	0.8092
CEBPB	1.4336	1.0564
CEBPD	0.8261	0.5665
KLF15	4.2002	7.8730
LEP	0.8650	0.7210
ADIPOQ	2.3432	1.2264
AP2B1	0.7541	0.9276
FOXO1	1.9200	1.4321
SLC2A4	1.2509	1.0284
RUNX2	0.4624	0.7576
FOS	0.7956	0.3422
JUN	0.6616	0.4266
STAT1	0.7229	0.7139
SMAD1	1.0395	1.3637
SP7	Adipose only	Adipose only
ALPL	10.6316	1.5629
PAX3	0.0563	Adipose only
PAX7	Adipose only	Adipose only
MEF2C	0.4435	1.2908
TBX5	0.2465	Adipose only
KDR	2.8002	Adipose only
CXCR4	ND	BM only
NKX2-5	Dermal only	ND

Endodermal		
	Adipose / Dermal	Adipose / BM
AFP	2.0655	0.5843
ALB	ND	BM only
CD44	1.0116	1.3584
CDH1	5.3242	1.3244
CDH2	5.8358	1.4388
CTNNA1	0.9106	0.7770
CTNNB1	0.8035	0.7119
CXCR4	ND	BM only
CYP7A1	Adipose only	Adipose only
FN1	0.9322	0.8965
HNF1A	1.3105	0.9468
HNF1B	1.3378	0.4668
HNF4A	Adipose only	0.3549
HTATSF1	0.9685	1.0462
ISL1	Adipose only	0.2334
ITGA6	0.1835	0.4860
ITGB1	0.7992	0.8514
KRT7	0.7876	0.9359
NRP2	1.0134	1.0528
OTX1	0.2428	2.8003
SYP	1.0983	0.7001
THY1	0.7876	0.9118
TTR	Dermal only	ND
GATA6	4.3770	1.3704

Ectodermal		
	Adipose / Dermal	Adipose / BM
SOX2	0.2190	0.4993
NEUROG2	ND	BM only
HES1	1.8092	0.2084
HES5	0.3344	0.2169
ASCL1	Dermal only	ND
ZNF521	1.2807	13.9544
NES	0.3800	4.6525
MSI1	Adipose only	0.7347
OLIG2	ND	BM only
ISL1	Adipose only	0.2334
ISL2	0.1484	0.1060
GFAP	0.8829	Adipose only
POU3F2	1.0385	3.6332
MYT1L	Adipose only	Adipose only
NR4A2	0.5149	0.0536
DLX1	1.9342	0.2784
DLX2	6.9419	0.4366
MAP2	0.3737	0.5471
TP63	0.1497	0.0956
CRABP2	0.1967	1.2002
FN1	0.9322	0.8965
NOTCH1	0.8426	1.3712
NGFR	0.2069	0.3905
S100B	Dermal only	BM only

Expression level in adipose-Muse cells that is higher than that in dermal- or BM-Muse cells is indicated by red, whereas lower is indicated by blue colors.
BM, bone marrow.
Color images available online at www.liebertpub.com/scd

directly contribute to cell replacement or tissue regeneration [24,25]. In the true sense of functional recovery, replenishment of functional cells is essential; however, the major consensus of the primary efficacy of adipose-MSC transplantation is also attributed to trophic effects [25]. This could be explained, in part, by the small percentage of adipose-Muse cells within adipose-MSC population. However, if the ratio of adipose-Muse cells could be increased, then there may be an improvement in the curative effect of adipose-MSC transplantation. Recently, Muse cells derived from adipose tissue were reported to have been efficiently enriched from human lipoaspirated fat by long-term incubation with collagenase. Such a simple approach would be an extremely practical strategy to increase the overall yield of Muse cells for stem cell therapy [26].

BM, dermis, and adipose tissue are representative mesenchymal sources for cell-based therapy because of their easy accessibility and versatility. Even though core properties of Muse cells, namely, triploblastic differentiation, self-renewal, nontumorigenicity, and surface marker expression, are the same among those three sources, Muse cells are not the same in their gene expression that relate to endodermal-, mesodermal-, and ectodermal-lineage differentiation. Adipose-Muse cells exhibited the tendency toward expressing mesodermal lineage genes more highly than BM- and dermal-Muse cells. Conversely, genes related to endodermal and ectodermal lineages were lower in adipose-Muse cells than in those two sources. Therefore, the source for Muse cells should be selected in accordance with target tissues.

Our data show that expression of human peroxisome proliferator-activated receptor gamma (PPARγ), a gene of mesodermal lineage, in adipose-Muse cells exceeds that of dermal- and BM-Muse cells. Considering that PPARγ expression is highly sensitive to the host environment, it may play a role in the unique adipose-Muse cell response to highly stressful conditions [27]. Other mesodermal genes that are elevated in adipose-Muse cells include Krüppel-like factor 15 (KLF15) and adiponectin (ADIPOQ), which encode prominent factors in adipocyte function, further supporting the preferential adipose-Muse cell differentiation to adipocytes [26].

Genes that are downregulated in adipose-Muse cells include FOS and JUN, genes that function paradoxically in both oncogenesis and tumor suppression depending on the cell type and its differentiation state and tumor stage [28]. CDH1, which encodes Cadherin-1, was expressed more highly in adipose-Muse cells than in BM- and dermal-Muse cells. Low expression of Cadherin-1 can support tumor progression, which may allude to the absence of tumorigenesis in CDH1-rich adipose-Muse cells [29]. Further, alpha-6 integrin (ITGA6) that plays a role in mammary tumorigenesis is decreased in adipose-Muse cells as compared with dermal- and BM-Muse cells [30]. Together with low telomerase activity and nontumorigenicity, this gene expression pattern may support the safety of adipose-Muse

cells for autologous transplantation. The uniqueness in the nontumorigenicity of Muse cells has been reported previously [16,17]. Gene analysis has shown that Muse cells exhibit extremely low expression of Lin28 [17], a gene that plays a pivotal role in both maintaining pluripotency and tumorigenesis that prevail in ES and iPS cells [31]. While Muse cells retain their pluripotent capacity in the absence of a Lin28 influence [17], they reap the benefits in their insusceptibility to tumor formation. Lin28 is likely only one of the many genes that simultaneously play a role in pluripotency as well as tumorigenesis, as these two prominent aspects of stem cell character have been repeatedly described to go hand-in-hand [26,31].

It is of significance to note that ectodermal genes are primarily downregulated in adipose-Muse cells as compared with dermal- and BM-Muse cells. Important genes in neural stem cell differentiation, including HES5 and achaete-scute homolog 1 (ASCL1), are poorly expressed in adipose-Muse cells. This may indicate, perhaps, a decrease in susceptibility to neural differentiation as compared with dermal- and BM-Muse cells. Interestingly, POU domain, class 3, transcription factor 2 (POU3F2), a gene that is imperative to differentiation of pluripotent stem cells into neural cells [32], is increased in adipose-Muse cells, which suggests a capacity of adipose-Muse cells to, if not a susceptibility to, neuronal differentiation.

There exists a cohort of genes that are present only in adipose-Muse cells, and not in dermal- and BM-Muse cells. Along the mesodermal lineage, adipose-Muse cells express SP7, which encodes transcription factor Sp7, and PAX7, which encodes paired box protein Pax7. SP7 regulates osteogenic differentiation [33] and the presence of SP7 in adipose-Muse cells but not in dermal- and BM-Muse cells suggests the high capacity of adipose-Muse cells to form bone cells. It has been shown that PAX7 plays a critical role in stem cell commitment to the myosatellite cell fate, which represents a niche for a population of quiescent stem cells that have the capacity for the regeneration of muscle tissue [34,35]. PAX7 could therefore be a critical factor in the maintenance of adipose-Muse cells to remain in quiescence [26]. Along the endodermal lineage, adipose-Muse cells express CYP7A1, which encodes cholesterol 7 alpha-hydroxylase and plays a major role in maintaining hepatocyte function [36]. This supports adipose-Muse cell aptitude for differentiation into functional hepatocytes. Along the ectodermal lineage, adipose-Muse cells express MYT1L, which encodes myelin transcription factor 1-like, and thus also support the possibly of differentiation into myelin-forming cells, such as oligodendrocytes [37].

Recently, a rare population of Lin−/CD75+/CD90− pluripotent stem cells was isolated from normal human breast tissue. Similar to adipose-Muse cells, this cell population has low telomerase activity [38]. While Lin−/CD75+/CD90− cells have low tumorigenicity, adipose-Muse cells have nontumorigenic activity. This difference may be attributable in part to the expression of CD90 in adipose-Muse cells. CD90, also known as THY1, is a classical marker for mesenchymal stem cells. The role of CD90 in promoting or suppressing tumorigenesis is still controversial likely depending on the tissue target analyzed [39,40].

Several reports have indicated the presence of a population of very small cells termed very small embryonic-like stem cells (VSELs) in BM or in circulation, which like Muse cells have been described to have pluripotent potential [41]. However, other labs have failed to replicate this data, with only one lab demonstrating that VSELs could differentiate to lung epithelium [42,43]. While Muse cells do not share morphologic or molecular markers with VSELs, the current controversy in VSELs regarding the reproducibility emphasizes the importance of having both simple and reproducible protocols as an essential aspects for the utilization of cells.

Since AT-MSCs exhibited a higher concentration of Muse cells and higher propensity for cluster formation than in LA-MSCs, Muse cells can be obtained from adipose tissue rather than commercially available adipose-MSCs. Based on our results, $\sim 15\,cm^3$ human adipose tissue (eg, $4 \times 9.5\,cm^2$ subcutaneous adipose tissue) yields $\sim 3 \times 10^7$ MSCs by week 3, which contain nearly $\sim 3 \times 10^6$ of adipose-Muse cells (corresponding to nearly 9% of total adipose-MSCs; see Supplementary Fig. S1 and Table 1). Granted that one million Muse cells are required for one-time treatment, the same volume of $\sim 15\,cm^3$ adipose tissue for 1 week culturing is estimated to be necessary. Interestingly, from 1 to 2 mL of BM, $\sim 3 \times 10^7$ MSCs can be obtained after 3 weeks that contain $\sim 0.3 \times 10^6$ BM-Muse cells ($\sim$1% of BM-MSCs). From these calculations, adipose-Muse cells can be considered a realistic cell source for regenerative medicine as with BM-Muse cells. Cell safety is the most important issue for the treatment of human disorders. Adipose-Muse cells do not require additional gene transfer or artificial modifications. They are naturally preexisting stem cells in adult human adipose tissue that account for a small percentage of adipose-MSCs, which have already been applied in clinical studies. Both the capacity for differentiation and lack of teratoma formation make adipose-Muse cells an attractive source for use in the clinical setting. However, there are still several hurdles that must be overcome on the way to making these cells a viable clinical resource, beyond what is already observed in adipose stem cells utilized in the clinical setting. Therefore, future experiments must include rigorous in vivo studies that explore the functional capability and nontumorigenicity of transplanted adipose-Muse cells, as well as further evidence of consistent and predictable controlled differentiation for various directed lineages.

Acknowledgment

This study was supported by the grant aid of New Energy and Industrial Technology Development Organization (NEDO).

Author Disclosure Statement

All authors state that they have no competing financial interests.

References

1. Zuk PA, M Zhu, P Ashjian, DA De Ugarte, JI Huang, et al. (2002). Human adipose tissue is a source of multipotent stem cells. Mol Biol Cell 13:4279–4295.
2. Cho YB, WY Lee, KJ Park, M Kim, HW Yoo, et al. (2013). Autologous adipose tissue-derived stem cells for the treat-

ment of Crohn's fistula: a phase I clinical study. Cell Transplant 22:279–285.
3. Tzouvelekis A, V Paspaliaris, G Koliakos, P Ntolios, E Bouros, et al. (2013). A prospective, non-randomized, no placebo-controlled, phase Ib clinical trial to study the safety of the adipose derived stromal cells-stromal vascular fraction in idiopathic pulmonary fibrosis. J Transl Med 11:171.
4. Gimble JM, AJ Katz and BA Bunnell. (2007). Adipose-derived stem cells for regenerative medicine. Circ Res 100:1249–1260.
5. Ikegame Y, K Yamashita, S Hayashi, H Mizuno, M Tawada, et al. (2011). Comparison of mesenchymal stem cells from adipose tissue and bone marrow for ischemic stroke therapy. Cytotherapy 13:675–685.
6. Boulland JL, M Mastrangelopoulou, AC Boquest, R Jakobsen, A Noer, et al. (2013). Epigenetic regulation of nestin expression during neurogenic differentiation of adipose tissue stem cells. Stem Cells Dev 22:1042–1052.
7. Kingham PJ, DF Kalbermatten, D Mahay, SJ Armstrong, M Wiberg, et al. (2007). Adipose-derived stem cells differentiate into a Schwann cell phenotype and promote neurite outgrowth *in vitro*. Exp Neurol 207:267–274.
8. Chandra V, G Swetha, S Muthyala, AK Jaiswal, JR Bellare, et al. (2011). Islet-like cell aggregates generated from human adipose tissue derived stem cells ameliorate experimental diabetes in mice. PLoS One 6: e20615.
9. Banas A, T Teratani, Y Yamamoto, M Tokuhara, F Takeshita, et al. (2007). Adipose tissue-derived mesenchymal stem cells as a source of human hepatocytes. Hepatology 46:219–228.
10. Ruiz JC, JW Ludlow, S Sherwood, G Yu, X Wu, et al. (2010). Differentiated human adipose-derived stem cells exhibit hepatogenic capability *in vitro* and *in vivo*. J Cell Physiol 225:429–436.
11. Aurich H, M Sgodda, P Kaltwasser, M Vetter, A Weise, et al. (2009). Hepatocyte differentiation of mesenchymal stem cells from human adipose tissue *in vitro* promotes hepatic integration *in vivo*. Gut 58:570–581.
12. Okura H, A Saga, Y Fumimoto, M Soeda, M Moriyama, et al. (2011). Transplantation of human adipose tissue-derived multilineage progenitor cells reduces serum cholesterol in hyperlipidemic Watanabe rabbits. Tissue Eng Part C Methods 17:145–154.
13. Chen J, YX Tang, YM Liu, XQ Hu, N Liu, et al. (2012). Transplantation of adipose-derived stem cells is associated with neural differentiation and functional improvement in a rat model of intracerebral hemorrhage. CNS Neurosci Ther 18:847–854.
14. Lee TH and JG Yoon. (2008). Intracerebral transplantation of human adipose tissue stromal cells after middle cerebral artery occlusion in rats. J Clin Neurosci 15:907–912.
15. Valina C, K Pinkernell, YH Song, X Bai, S Sadat, et al. (2007). Intracoronary administration of autologous adipose tissue-derived stem cells improves left ventricular function, perfusion, and remodelling after acute myocardial infarction. Eur Heart J 28:2667–2677.
16. Kuroda Y, M Kitada, S Wakao, K Nishikawa, Y Tanimura, et al. (2010). Unique multipotent cells in adult human mesenchymal cell populations. Proc Natl Acad Sci USA 107:8639–8643.
17. Wakao S, M Kitada, Y Kuroda, T Shigemoto, D Matsuse, et al. (2011). Multilineage-differentiating stress-enduring (Muse) cells are a primary source of induced pluripotent stem cells in human fibroblasts. Proc Natl Acad Sci USA 108:9875–9880.
18. Pittenger MF, AM Mackay, SC Beck, RK Jaiswal, R Douglas, et al. (1999). Multilineage potential of adult human mesenchymal stem cells. Science 284:143–147.
19. Dezawa M, H Kanno, M Hoshino, H Cho, N Matsumoto, et al. (2004). Specific induction of neuronal cells from bone marrow stromal cells and application for autologous transplantation. J Clin Invest 113:1701–1710.
20. Estes BT, BO Diekman, JM Gimble and F Guilak. (2010). Isolation of adipose-derived stem cells and their induction to a chondrogenic phenotype. Nat Protoc 5:1294–1311.
21. Kuroda Y, S Wakao, M Kitada, T Murakami, M Nojima, et al. (2013). Isolation, culture and evaluation of multilineage-differentiating stress-enduring (Muse) cells. Nat Protoc 8:1391–1415.
22. Livak KJ and TD Schmittgen. (2001). Analysis of relative gene expression data using real-time quantitative PCR and the 2(-Delta Delta C(T)) Method. Methods 25:402–408.
23. Gimble J and F Guilak. (2003). Adipose-derived adult stem cells: isolation, characterization, and differentiation potential. Cytotherapy 5:362–369.
24. Venkataramana NK, SK Kumar, S Balaraju, RC Radhakrishnan, A Bansal, et al. (2010). Open-labeled study of unilateral autologous bone-marrow-derived mesenchymal stem cell transplantation in Parkinson's disease. Transl Res 155:62–70.
25. Ren G, X Chen, F Dong, W Li, X Ren, et al. (2012). Concise review: mesenchymal stem cells and translational medicine: emerging issues. Stem Cells Transl Med 1: 51–58.
26. Heneidi S, AA Simerman, E Keller, P Singh, X Li, et al. (2013). Awakened by cellular stress: isolation and characterization of a novel population of pluripotent stem cells derived from human adipose tissue. PLoS One 8: e64752.
27. Greene ME, J Pitts, MA McCarville, XS Wang, JA Newport, et al. (2000). PPARgamma: observations in the hematopoietic system. Prostaglandins Other Lipid Mediat 62:45–73.
28. Eferl R and EF Wagner. (2003). AP-1: a double-edged sword in tumorigenesis. Nat Rev Cancer 3:859–868.
29. Ceteci F, S Ceteci, C Karreman, BW Kramer, E Asan, et al. (2007). Disruption of tumor cell adhesion promotes angiogenic switch and progression to micrometastasis in RAF-driven murine lung cancer. Cancer Cell 12:145–159.
30. Ali HR, SJ Dawson, FM Blows, E Provenzano, PD Pharoah, et al. (2011). Cancer stem cell markers in breast cancer: pathological, clinical and prognostic significance. Breast Cancer Res 13: R118.
31. Thornton JE and RI Gregory. (2012). How does Lin28 let-7 control development and disease? Trends Cell Biol 22: 474–482.
32. Pang ZP, N Yang, T Vierbuchen, A Ostermeier, DR Fuentes, et al. (2011). Induction of human neuronal cells by defined transcription factors. Nature 476:220–223.
33. Nakashima K, X Zhou, G Kunkel, Z Zhang, JM Deng, et al. (2002). The novel zinc finger-containing transcription factor osterix is required for osteoblast differentiation and bone formation. Cell 108:17–29.
34. Kadi F, P Schjerling, LL Andersen, N Charifi, JL Madsen, et al. (2004). The effects of heavy resistance training and detraining on satellite cells in human skeletal muscles. J Physiol 558:1005–1012.

35. Relaix F, D Rocancourt, A Mansouri and M Buckingham. (2005). A Pax3/Pax7-dependent population of skeletal muscle progenitor cells. Nature 435:948–953.
36. Cohen JC, JJ Cali, DF Jelinek, M Mehrabian, RS Sparkes, et al. (1992). Cloning of the human cholesterol 7 alpha-hydroxylase gene (CYP7) and localization to chromosome 8q11-q12. Genomics 14:153–161.
37. Ambasudhan R, M Talantova, R Coleman, X Yuan, S Zhu, et al. (2011). Direct reprogramming of adult human fibroblasts to functional neurons under defined conditions. Cell Stem Cell 9:113–118.
38. Roy S, P Gascard, N Dumont, J Zhao, D Pan, et al. (2013). Rare somatic cells from human breast tissue exhibit extensive lineage plasticity. Proc Natl Acad Sci USA 110: 4598–4603.
39. Abeysinghe HR, Q Cao, J Xu, S Pollock, Y Veyberman, et al. (2003). THY1 expression is associated with tumor suppression of human ovarian cancer. Cancer Genet Cytogenet 143:125–132.
40. He J, Y Liu, T Zhu, J Zhu, F Dimeco, et al. (2012). CD90 is identified as a candidate marker for cancer stem cells in primary high-grade gliomas using tissue microarrays. Mol Cell Proteomics 11: M111 010744.
41. Drukala J, E Paczkowska, M Kucia, E Mlynska, A Krajewski, et al. (2012). Stem cells, including a population of very small embryonic-like stem cells, are mobilized into peripheral blood in patients after skin burn injury. Stem Cell Rev 8:184–194.
42. Kassmer SH, H Jin, PX Zhang, EM Bruscia, K Heydari, et al. (2013). Very small embryonic-like stem cells from the murine bone marrow differentiate into epithelial cells of the lung. Stem Cells. [Epub ahead of print]; DOI: 10.1002/stem.1413.
43. Miyanishi M, Y Mori, J Seita, JY Chen, S Karten, et al. (2013). Do pluripotent stem cells exist in adult mice as very small embryonic stem cells? Stem Cell Rep 1:198–208.

Address correspondence to:
Prof. Mari Dezawa
Department of Stem Cell Biology and Histology
Tohoku University Graduate School of Medicine
2-1 Seiryo-machi, Aoba-ku
Sendai 980-8575
Japan

E-mail: mdezawa@med.tohoku.ac.jp

Received for publication September 28, 2013
Accepted after revision November 18, 2013
Prepublished on Liebert Instant Online November 20, 2013

Vasculogenesis in Experimental Stroke After Human Cerebral Endothelial Cell Transplantation

Hiroto Ishikawa, MD, PhD; Naoki Tajiri, PT, PhD; Kazutaka Shinozuka, PhD; Julie Vasconcellos, BS; Yuji Kaneko, PhD; Hong J. Lee, PhD; Osamu Mimura, MD, PhD; Mari Dezawa, MD, PhD; Seung U. Kim, MD, PhD; Cesar V. Borlongan, PhD

Background and Purpose—Despite the reported functional recovery in transplanted stroke models and patients, the mechanism of action underlying stem cell therapy remains not well understood. Here, we examined the role of stem cell–mediated vascular repair in stroke.

Methods—Adult rats were exposed to transient occlusion of the middle cerebral artery and 3 hours later randomly stereotaxically transplantated with 100K, 200K, or 400K human cerebral endothelial cell 6 viable cells or vehicle. Animals underwent neurological examination and motor test up to day 7 after transplantation then euthanized for immunostaining against neuronal, vascular, and specific human antigens. A parallel in vitro study cocultured rat primary neuronal cells with human cerebral endothelial cell 6 under oxygen-glucose deprivation and treated with vascular endothelial growth factor (VEGF) and anti-VEGF.

Results—Stroke animals that received vehicle infusion displayed typical occlusion of the middle cerebral artery–induced behavioral impairments that were dose-dependently reduced in transplanted stroke animals at days 3 and 7 after transplantation and accompanied by increased expression of host neuronal and vascular markers adjacent to the transplanted cells. Some transplanted cells showed a microvascular phenotype and juxtaposed to the host vasculature. Infarct volume in transplanted stroke animals was significantly smaller than vehicle-infused stroke animals. Moreover, rat neurons cocultured with human cerebral endothelial cell 6 or treated with VEGF exhibited significantly less oxygen-glucose deprivation–induced cell death that was blocked by anti-VEGF treatment.

Conclusions—We found attenuation of behavioral and histological deficits coupled with robust vasculogenesis and neurogenesis in endothelial cell–transplanted stroke animals, suggesting that targeting vascular repair sets in motion a regenerative process in experimental stroke possibly via the VEGF pathway. **(*Stroke*. 2013;44:3473-3481.)**

Key Words: endothelial cells ■ neurogenesis ■ stem cells ■ stroke

Stem cell therapy has reached limited clinical trials in patients with stroke on the basis of safety and efficacy data from preclinical studies.[1–4] However, a major gap in our knowledge is the mechanism of action underlying stem cell therapy. Cell transplantation studies in stroke have mostly focused on neuronal stem or progenitor cells as donor cell type,[5–15] primarily to replace the dead or injured neuronal cells of the stroke brain. Indeed, such transplantation of neuronal stem or progenitor cells has resulted in neurogenesis with reported functional recovery in transplanted stroke animals.[5–15] Despite these positive observations, varying levels of behavioral and histological improvement accompany transplanted stroke animals. We posit that while new neurons have been generated from the either exogenously transplanted stem cells or transplant-mediated solicitation of endogenous stem cells, a key component of the neurovascular unit that has been largely neglected is the repair of the vasculature. To this end, we tested the hypothesis that stem cell transplantation in stroke using endothelial cells, which are the main cell type of the vasculature, should promote vasculogenesis and then likely serve as substrate for enhanced endogenous neurogenesis.

During the neurodevelopmental period, vasculogenesis and neurogenesis seem to occur at the same time,[16–18] suggesting that these 2 cell lineage processes are critical. Recently, the important role of endothelial cells in regulating both vasculogenesis and neurogenesis has been recognized.[19–22] Cerebral endothelial cells serve many cerebrovascular maintenance functions, including structural element, blood brain barrier

Received May 6, 2013; accepted September 4, 2013.

From the Department of Neurosurgery and Brain Repair, University of South Florida College of Medicine, Tampa, FL (H.I., N.T., K.S., J.V., Y.K., C.V.B.); Department of Ophthalmology, Hyogo College of Medicine, Nishinomiya, Japan (H.I., O.M.); Medical Research Institute, Chung-Ang University College of Medicine, Seoul, Korea (H.J.L.); Department of Stem Cell Biology and Histology and Department of Anatomy and Anthropology, Tohoku University Graduate School of Medicine, Sendai, Japan (M.D.); and Department of Neurology, University of British Columbia, Vancouver, British Columbia, Canada (S.U.K.).

The online-only Data Supplement is available with this article at http://stroke.ahajournals.org/lookup/suppl/doi:10.1161/STROKEAHA.113.001943/-/DC1.

Correspondence to Cesar V. Borlongan, PhD, Department of Neurosurgery and Brain Repair, University of South Florida, 12901 Bruce B. Downs Blvd MDC78, Tampa, FL 33612. E-mail cborlong@health.usf.edu

Stroke **is available at http://stroke.ahajournals.org** **DOI: 10.1161/STROKEAHA.113.001943**

formation, regulation of neurotransmitter and ion, and controlling of blood flow.[23,24] Interestingly, these same cerebrovascular functions are compromised after ischemic stroke. If therapies could be designed to protect the brain vasculature from stroke-induced alterations, then we should be able to reduce the pathophysiological outcomes of stroke. Hence, the present study sought to engage the endothelial cell component of the neurovascular unit in an effort to abrogate stroke.

The potential therapeutic benefits of transplanting exogenous or mobilizing endogenous endothelial progenitor cells in stroke animal models have been demonstrated,[25,26] but the mechanisms remain not well understood. In this study, we transplanted the immortalized cell line of human cerebral endothelial cells (HEN6) into the striatum of experimentally ischemic stroke rats and assessed endogenous and exogenous vasculogenesis and neurogenesis to demonstrate the role of vascular repair in stroke. We hypothesized that transplantation of endothelial cells would afford behavioral and histological benefits against stroke via the vasculogenic reparative pathway in facilitating the neurogenic regenerative process.

Material and Methods

In Vivo Study

Subjects

We used adult Sprague–Dawley rats (weighing, 200–250 g at the beginning of experiments; Harlan Sprague Dawley, Indianapolis, IN) according to the approved guidelines of the University of South Florida System Institutional Animal Care and Use Committee. They were housed singly in a temperature and humidity controlled room that was maintained on 12-hour light/dark cycles with free access to food and water. All surgical procedures were conducted under aseptic conditions, and every effort was made to minimize animal suffering and to reduce the number of animals used.

Human Cerebral Endothelial Cells

HEN6 were kindly provided by Dr Kim (University of British Columbia, Vancouver, BC, Canada). Briefly, primary dissociated cell cultures from the periventricular region of human telencephalic tissues of 14-week gestation were prepared and grown for 10 days. Thereafter, cells were infected with an amphotropic, replication-incompetent retroviral vector containing v-myc. Finally, HEN6 were subcultured at ≈90% confluence and subjected to further experiments. Next, we phenotypically characterized HEN6 in vitro and found that these cells were immunocytochemically positive against a human mitochondrial marker (Mito), von Willebrand factor (vWF), and CD31 that the positivity was >99% for each phenotypic marker (Figure 1).

Stroke Surgery

The present ischemic stroke model used the middle cerebral artery occlusion (MCAo) technique as described in our previous studies.[27–30] We used 46 rats for the surgery, and 40 rats reaching our criterion of successful MCAo, as described elsewhere, were enrolled in the study. Briefly, animals were anesthetized by a mixture of 1% to 2% isofluran in NO/oxygen (69%/30%) via a face mask. Body temperature was maintained at 37±0.3°C during the surgical procedures. The midline skin incision was made in the neck with subsequent exploration of the right common carotid artery, the external carotid artery, and internal carotid artery. A 4-0 monofilament nylon suture (27.0–28.0 mm) was advanced from the common carotid artery bifurcation until it blocked the origin of the MCA. Animals were allowed to recover from anesthesia during MCAo. After 60 minutes of transient MCAo, animals were reanesthetized and reperfused by withdrawal of the nylon thread. Animals receiving the sham operation were anesthetized with the same gas via a face mask. A midline incision was made in the neck and the right common carotid artery was isolated. The animals were then closed and allowed to recover from anesthesia. We have standardized the MCAo model, with stroke animals showing ≥80% reduction in regional cerebral blood flow during the occlusion period as determined by laser Doppler (Perimed). To ensure further similar degree of stroke insults, physiological parameters, including Pao_2, $PaCO_2$, and plasma PH measurements, were monitored, and we found no significant differences in our stroke animals.

HEN6 Cells Transplantation

Forty rats (n=10 for each group) were randomly assigned to receive stereotaxic transplantation of PBS as a control, 100K, 200K, or 400K HEN6/9 μL, 3 hours after MCAo. Transplantation targeted the striatum via a single Hamilton (25 gauge) needle pass with 3 dorsoventral deposits (bregma, +1.2 mm; medial-lateral, +2.5 mm; dorsal-ventral, −5.0/−4.5/−4.0 mm).[31]

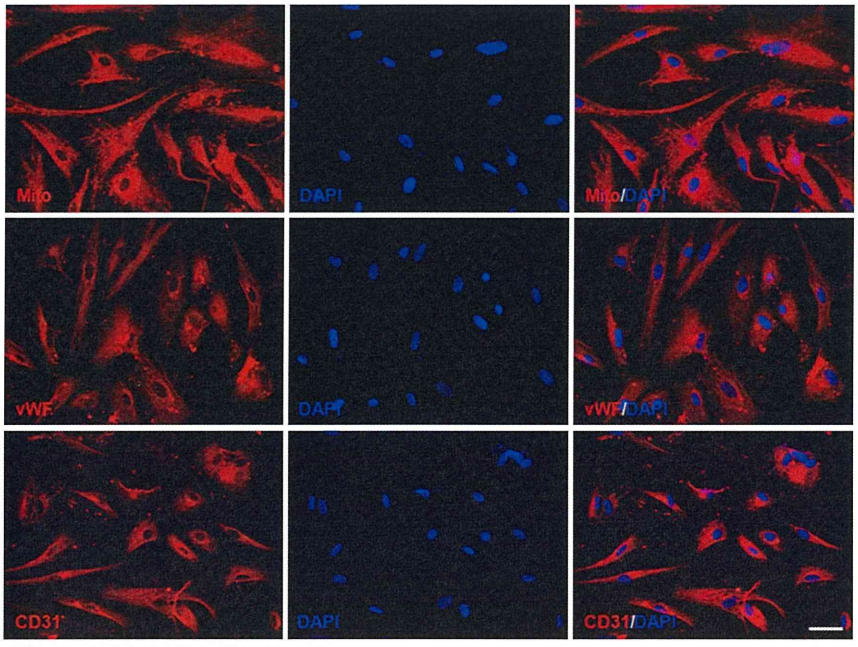

Figure 1. Immunocytochemical analysis of human cerebral endothelial cells (HEN6), immortalized HEN6, immunocytochemically expressed human-specific mitochondrial marker (Mito), von Willebrand factor (vWF), and CD31. DAPI indicates 4',6-diamidino-2-phenylindole.

Motor and Neurological Tests

All investigators testing the animals were blinded to the treatment condition. Animals were subjected to elevated body swing test and neurological examination before stroke surgery (baseline) then at days 3, 5, and 7 after surgery. Elevated body swing test involved handling the animal by its tail and recording the direction of the swings. The test apparatus consisted of a clear Plexiglas box (40×40×35.5 cm). The animal was gently picked up at the base of the tail and elevated by the tail until the animal's nose is at a height of 2 inches (5 cm) above the surface. The direction of the swing, either left or right, was counted once the animals head moves sideways ≈10° from the midline position of the body. These steps are repeated 20× for each animal. Intact rats displayed a 50% swing bias (ie, the same number of swings to the left and to the right). A 75% swing bias was used as a criterion of stroke-induced motor asymmetry. Animals were also tested in a modified neurological examination. Neurological score for each rat was obtained using 3 tests that included (1) forelimb akinesia that measured the ability of the animal to replace the forelimb after it was displaced laterally by 2 to 3 cm, graded from 0 (immediate replacement) to 3 (replacement after several seconds or no replacement); (2) beam walking ability, graded 0 for a rat that readily traversed a 2.4-cm-wide, 80-cm-long beam to 3 for a rat unable to stay on the beam for 10 seconds; and (3) paw grasp that measured the ability to hold onto a 2-mm-diameter steel rod, graded 0 for a rat with normal forepaw grasping behavior to 3 for a rat unable to grasp with the forepaws. The scores from this battery of 3 neurological tests were pooled to obtain the mean neurological score for each treatment group. A ≥2.5 mean neurological score was used as a criterion of stroke-induced neurological impairment.

Histology and Immunohistochemistry

Twenty-four rats (n=6 for each group) were deeply anesthetized and perfused transcardially with 4% paraformaldehyde 7 days after HEN6 transplantation. Brains were harvested and postfixed in the same fixative for 24 hours followed by 30% sucrose in PBS for 1 week. Frozen sections were then cut at 30 μm in a cryostat and stored at −20°C. To demonstrate graft survival, neuronal and vascular phenotype expression and immunohistochemical investigations were performed. Free-floating sections throughout the transplanted striatum and continuing cortex involving the stroke area were incubated overnight at 4°C with an anti-nestin antibody (mouse; anti-nestin antibody [ab6142]; abcam), glial fibrillary acidic protein (GFAP) (mouse, anti-GFAP antibody [MAB360]; Millipore), collagen IV (rabbit, anti-collagen IV antibody [ab19808]; abcam), and HuNu (mouse, anti-human nuclei antibody [MAB1281]; Millipore) for engrafted HEN6, with 5% serum and 0.2% triton X-100 (Fischer Scientific, Pittsburgh, PA). After rinsing 3× in PBS, sections were incubated for 2 hours at room temperature in goat antimouse IgG Alexa Fluor 488 conjugate (Invitrogen) and goat anti-rabbit IgG Alexa Fluor 594 conjugate (Invitrogen) with Hoechst33342 (Sigma). Next, the sections were washed again 3× in PBS and mounted on glass slides using mounting medium. Control studies included exclusion of primary antibody substituted with 10% goat serum in PBS. No immunoreactivity was observed in these controls.

HEN6 Graft Survival Assessment

For evaluation of graft survival, HuNu-positive cells were counted every fifth 30-μm-thick coronal tissue section throughout the transplanted striatum by an observer blinded to the experimental group assignment. Abercrombie formula was used to eliminate bias of counting the same cell in 2 consecutive sections.

Infarct Measurement

The remaining 16 rats (n=4 for each group) were euthanized at 7 days PBS or HEN6 transplantation. Coronal sections of the brains were sliced at 2 mm, immersed in 2% 2,3,5-triphenyltetrazolium chloride (TTC; T8877; Sigma), and then fixed with 4% paraformaldehyde. The size of infarct area, which was devoid of red staining, was determined on the digital images using ImageJ software and calculated the ratio of infarct area toward whole brain by an observer blinded to the experimental group assignment as described in our reports.[7,29,30]

Analysis of Glial Formation and Blood Vessels

As described above, cryosections were processed for immunohistochemical staining against GFAP for glial formation and collagen IV for blood vessels. Glial formation is defined as the proportion of the area occupied by GFAP-positive cells, which was calculated every fifth 30-μm-thick coronal tissue section throughout the stroke striatal penumbra. In a similar fashion, we measured vessel density defined as the proportion of the area occupied by collagen IV–positive area in the striatum. They were measured using ImageJ software by an observer blinded to the experimental group assignment.

In Vitro Study

Vascular Endothelial Growth Factor Role in Oxygen-Glucose Deprivation

Primary rat neonatal neuronal cells (PRNCs) were obtained from BrainBit. According to the supplier protocol, cells (4×10^4 cells/well) were suspended in 200-μL supplemented neurobasal medium containing 2-mmol/L L-glutamine and 2% B27 in the absence of antibiotics and grown in poly-L-Lysine–coated 96-well plate (BD Biosciences) at 37°C in humidified atmosphere containing 5% carbon dioxide in 40% of the neuron and 60% astrocytes cell population and validated immunocytochemically using vesicular glutamate transporter-1. PRNCs were grown until reaching cell confluence of ≈70% then subjected to 90-minute oxygen-glucose deprivation (OGD) as described previously.[32] Briefly, the PRNCs were initially exposed to OGD medium (116 mmol/L NaCl, 5.4 mmol/L KCl, 0.8 mmol/L $MgSO_4$, 1 mmol/L NaH_2PO_4, 26.2 mmol/L $NaHCO_3$, 0.01 mmol/L glycine, 1.8 mmol/L $CaCl_2$; pH 7.4) and placed in an anaerobic chamber (PlasLabs) containing 95% nitrogen and 5% carbon dioxide for 15 minutes at 37°C, and finally the chamber was sealed and incubated for 90 minutes at 37°C (hypoxic-ischemic condition). After the hypoxic-ischemic exposure, the cell culture was reintroduced to reperfusion-like condition containing 5 mmol/L glucose under normoxia for 2 hours.

To reveal the involvement of vascular endothelial growth factor (VEGF) in HEN6 neuroprotection, we initially examined the therapeutic benefits of exogenous VEGF by manipulating the basal medium when the reperfusion started (Figure I in the online-only Data Supplement) as follows: group A: basal medium as a control; group B: low concentration (0.5 ng/mL) of VEGF; group C: high concentration (5.0 ng/mL) of VEGF; group D: group A with anti-VEGF; group E: group B with anti-VEGF; and group F: group C with anti-VEGF. Two hours after the reperfusion, the supernatant was collected from the culture and the PRNCs were subjected to the mitochondrial activity assay. For the mitochondrial activity assay, reduction of 3-(4, 5-dimethyl-2-thiazoyl)-2,5-diphenyltetrazolium bromide (MTT) by cellular dehydrogenases was used as described in our previous report.[33]

Coculture of Neuronal Cells After the OGD Condition With HEN6 or Fibroblasts

HEN6 and fibroblasts, as control cells, were separately grown to a subconfluent monolayer in 10-cm dishes, and then they were rinsed twice with PBS before being plated in culture plate inserts (3-μm membrane pore size; BD Biosciences). In parallel, the 4×10^4 of PRNCs were plated in 96-well companion plates (BD Biosciences) and subjected to 90-minute OGD condition. After the OGD condition for PRNCs, the inserts containing HEN6 and fibroblasts were transferred to these wells, and the coculture was introduced to one of the conditions (Figure I in the online-only Data Supplement) in the normoxic incubator for 2 hours (these conditions corresponded to reperfusion with or without VEGF and anti-VEGF). The coculture was assigned to further experiments. Before cell viability analyses, the culture plate inserts containing HEN6 or fibroblast were removed, and then we used the bottom of the plate cultured with only neuronal cells for analyses.

For the neuronal cell viability, we used the fluorescent live/dead cell assay.[34] The green fluorescence of the live cells was measured

by the Gemini EX fluorescence plate reader (Molecular Device). To evaluate the VEGF levels in the supernatants collected from pre and post reperfusion process, we used ELISA VEGF detection kits (R&D systems). To reveal the localization of damaged cells, we examined immunocytochemical against caspase 3.

Statistical Analysis

We used repeated ANOVA followed by Fisher protected least significant difference post hoc tests to reveal any statistical significance between treatments ($P<0.05$). All data were presented as mean±SEM. In addition, Pearson R coefficient of correlation was performed to show interactions between neuroprotective mechanisms and functional recovery. In the statistical analyses of in vitro data, because of the differences in the baseline of treatment conditions, basal media data were normalized among single culture, coculture with basal media, and coculture with HEN6.

Results

Transplanted HEN6 Cells Survive Dose Dependently in Stroke Brain

To reveal transplanted HEN6 survival, we used immunohistochemical detection of the specific human antigen HuNu. The number of HuNu-positive cells per visual field in 400K group (106.9±43.3) was significantly higher than that in 200K (70.4±31.7) and 100K (34.8±23.6) transplanted groups ($P<0.05$; Figure II in the online-only Data Supplement), thus the number of surviving transplanted HEN6 was dose dependent. However, the percentage of survival was comparable and not significantly different across all transplanted animals: 400K (0.23±0.08%), 200K (0.26±0.12%), 100K (0.26±0.18%).

HEN6 Transplantation Dose Dependently Ameliorates Stroke-Induced Behavioral Deficits

All animals included in this study did not display any detectable behavioral deficits at baseline (Figure 2). After MCAo stroke surgery, animals exhibited significant impairments in both motor and neurological performance, which were evident during the 1-hour MCAo (data not shown), and was maintained throughout the 7-day study period in those stroke animals that received vehicle infusion. In contrast, stroke animals that received HEN6 exhibited a dose-dependent improvement in behavioral outcomes (pairwise comparisons between groups, $P<0.05$), with the highest dose of 400K displaying the most pronounced functional recovery ($F_{4,26}=83.26$; $P<0.01$). This dose-dependent behavioral recovery was consistent for both motor and neurological assays and across all times points examined (ie, days 3, 5, and 7). Sham-operated animals (normal) did not show any detectable deficits throughout the study period. The HEN6 transplanted stroke animals, while demonstrating 20% to 45% improvement versus the vehicle-infused stroke animals, were still significantly impaired compared with this normal group ($P<0.05$).

HEN6 Transplantation Reduces Infarct Volume, Suppresses Reactive Gliosis, and Induces Vasculogenesis

We used TTC to determine the therapeutic effect of HEN6 on the brain infarct. The infarct volumes (total, in cortex, and in transplanted striatum) were 87.7±17.4 (27.1±5.4%), 57.4±11.1,

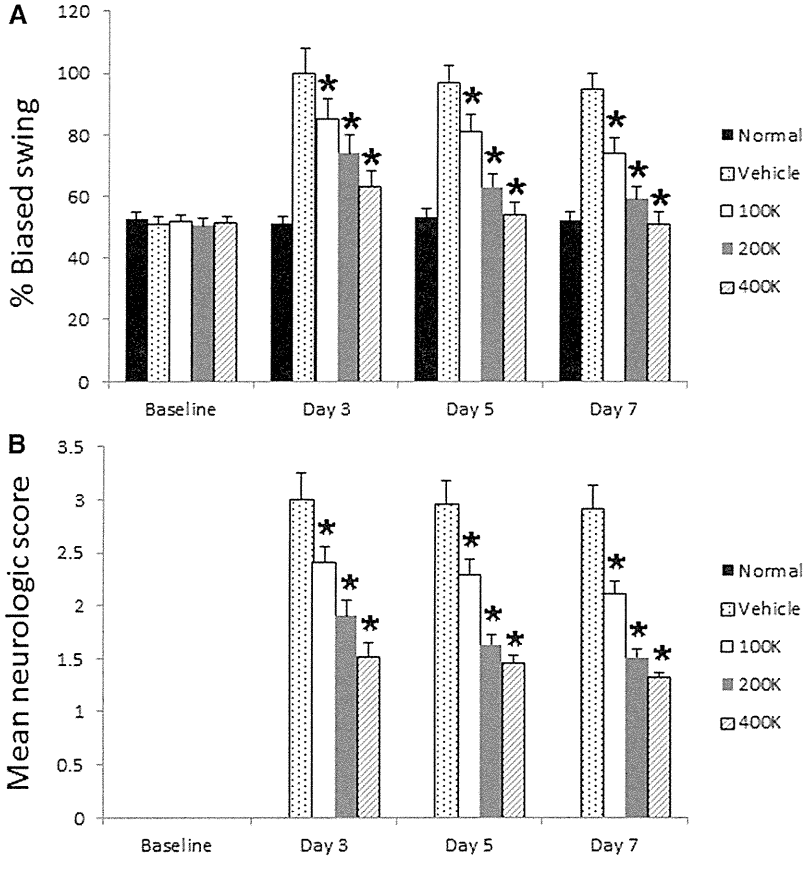

Figure 2. Human cerebral endothelial cells (HEN6) ameliorates stroke-induced behavioral deficits. All animals enrolled in this study displayed no detectable behavioral deficits at baseline, with sham-operated animals (normal) exhibiting normal behaviors throughout the study period. After middle cerebral artery occlusion stroke surgery throughout the 7-day study period, stroke animals that received vehicle infusion displayed significant motor (**A**) and neurological impairments (**B**). In contrast, dose-dependent improvements across all times points in both behavioral outcomes were displayed by stroke animals transplanted with HEN6, with the highest dose of 400K most improved. The HEN6 transplanted stroke animals, although significantly improved compared with the vehicle-infused stroke animals, were still significantly impaired compared with the normal group (*$P<0.05$).

and 30.2±9.6 mm^3 in control; 73.2±14.1 (23.9±3.1%), 52.8±8.0, and 20.4±10.0 mm^3 in 100K group; 40.4±15.8 (13.1±4.5%), 32.4±7.7, and 8.0±9.2 mm^3 in 200K group; and 30.8±14.3 (10.4±4.7%), 27.1±11.0, and 3.7±3.4 mm^3 in 400K group (Figure 3). The infarct volume was significantly reduced in 400K and 200K HEN6 transplanted groups compared with control group, which received PBS injection (P<0.05). Next, we used GFAP immunostaining to reveal reactive gliosis on peri-infarct area. The intensity ratio of GFAP-positive area in control, 100K, 200K, and 400K was 29.5±10.0, 26.7±9.2, 12.7±2.5, and 13.3±4.6% (Figure 3). Glial formation was significantly reduced in 400K and 200K HEN6 transplanted groups compared with 100K and control groups (P<0.05). In addition, we used collagen IV immunostaining to reveal vascularization within the area of the transplanted striatum. The intensities of collagen IV–positive area in control, 100K, 200K, and 400K were 0.2±0.3%, 6.3±6.9%, 18.2±10.7%, and 25.4±9.3% (Figure 3). Vasculogenesis within the striatum was significantly increased in 400K and 200K HEN6 transplanted groups compared with 100K and control groups (P<0.01).

HEN6-Mediated Neuroprotective Cellular Processes Correlate With Infarct Volume and Reactive Gliosis

All brain repair parameters, including survival of transplanted cells, reduction in infarct volume, suppression of gliosis change, and enhanced vasculogenesis, showed good correlations. The dose-dependent survival of transplanted cells correlated with infarct volume, gliosis (GFAP immunoreactivity), and vasculogenesis (collagen IV immunoreactivity; Figure 3B). The correlation matrix of these brain repair parameters showed positive correlations between infarct

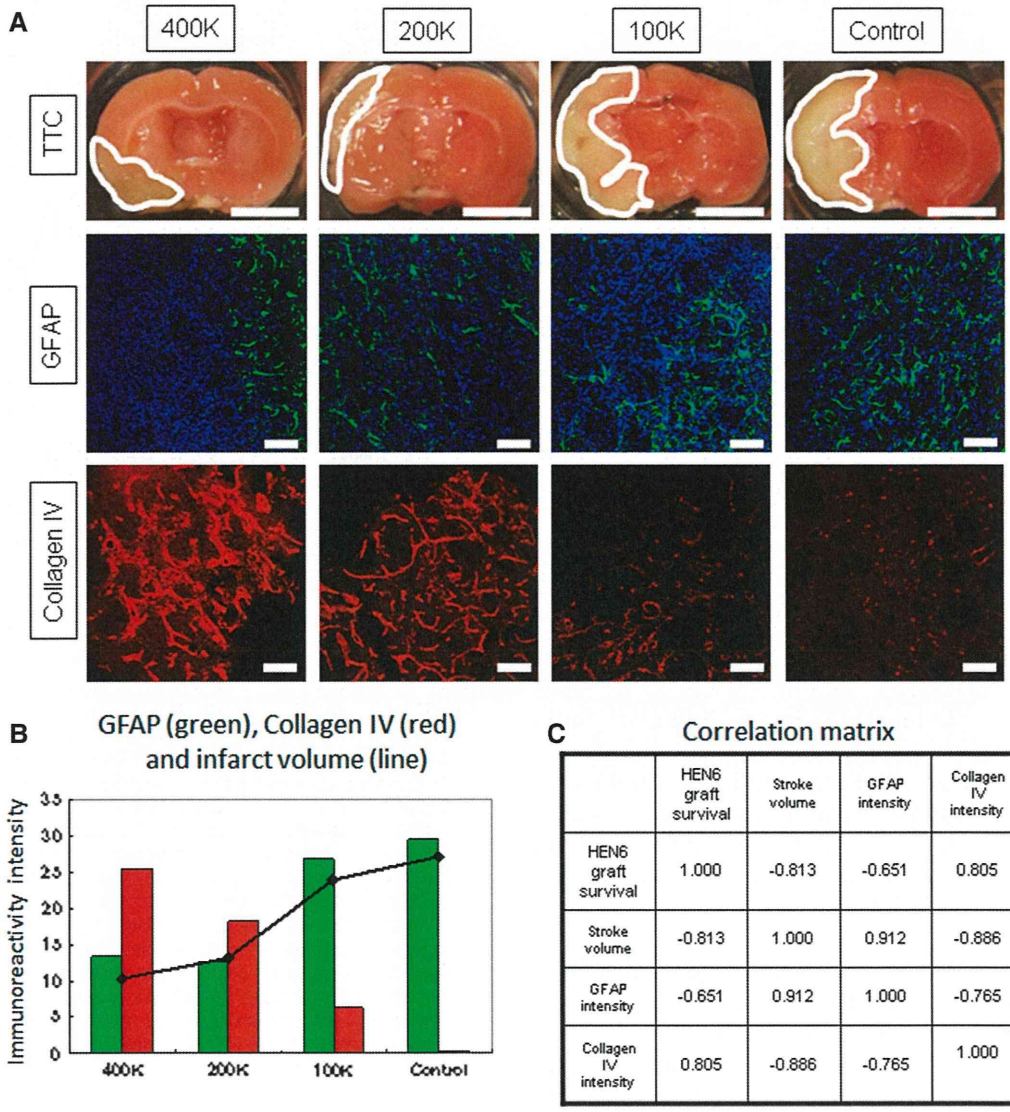

	HEN6 graft survival	Stroke volume	GFAP intensity	Collagen IV intensity
HEN6 graft survival	1.000	-0.813	-0.651	0.805
Stroke volume	-0.813	1.000	0.912	-0.886
GFAP intensity	-0.651	0.912	1.000	-0.765
Collagen IV intensity	0.805	-0.886	-0.765	1.000

Figure 3. Human cerebral endothelial cells (HEN6) attenuates stroke-induced histological deficits. Transplantation of HEN6 reduced infarct volume (2,3,5-triphenyltetrazolium chloride [TTC]), suppressed reactive gliosis (GFAP), and induced vasculogenesis (collagen IV; **A**). Graphical rendition of correlations among GFAP (green), collagen IV (red), and infarct volume (line) are presented (**B**), indicating that with HEN6 reducing the infarct volumes in 400K and 200K transplanted stroke animals, there was a corresponding suppression of reactive gliosis (GFAP) and elevation of collagen IV. Numeric coefficients of correlation are shown (**C**). Scale bar in TTC-stained brains is 5 mm. Scale bar in GFAP and collagen IV equals 50 μm. GFAP indicates glial fibrillary acidic protein.

volume and gliosis and a negative correlation between the infarct volume and the vasculogenesis. In addition, the correlation matrix showed that HEN6 graft survival was positively correlated with vasculogenesis but negatively correlated with gliosis, and gliosis was negatively correlated with vasculogenesis (Figure 3C).

HEN6 Induces Vasculogenesis in Endogenous and Exogenous Cells

To answer the question whether transplanted HEN6 afford neovascularization, we used double-immunolabeling of HuNu and collagen IV in the stroke brain. Surviving HuNu-positive transplanted HEN6 in ischemic striatum formed a new microvascular-like structure that was positive against collagen IV and juxtaposed to the host vasculature that was also positively stained against collagen IV (Figure 4). The formation of this microvascular-like structure was dose dependent, reflecting the dose-dependent HEN6 graft survival.

HEN6 Promotes Endogenous Neurogenesis

To reveal whether the HEN6 histological benefits extend to neurogenesis, we used double-immunolabeling of HuNu and nestin in the stroke brain. Nestin-positive cells were detected migrating from centrally located HuNu-positive–transplanted cells. In addition, colocalization of nestin-positive cells around HuNu-positive cells was observed (Figure 4).

VEGF Protects PRNCs Against OGD Condition

We examined cultured PRNCs with VEGF treatment under OGD condition as a prelude to assessing a VEGF role in HEN6 neuroprotection in stroke. The number of apoptotic caspase 3–positive cells in both VEGF treatment group (groups B [41.47±4.39%] and C [44.85±7.85%]) was significantly reduced than no VEGF treatment group [group A [59.15±8.62%]). Treatment with anti-VEGF in combination with VEGF in groups E (66.28±3.89%) and F (61.97±9.84%) abolished the VEGF neuroprotective effect ($P<0.05$). Moreover, anti-VEGF treatments alone (without VEGF; group D [89.75±3.92%]) significantly exacerbated the OGD-induced neurotoxicity compared with other groups ($P<0.05$; Figures I and V in the online-only Data Supplement). Relative mitochondrial reductase activity in VEGF treatment group (groups B [32.72±2.47%] and C [35.3±1.13%]) was significantly higher than in the basal medium (group A [25.77±0.57%]) and anti-VEGF treatment groups (groups D [13.35±2.21], E [16.02±1.45], and F [18.52±2.62%]; $P<0.05$; Figure 5).

Coculture of PRNCs and HEN6 Combined With VEGF Treatment Optimally Attenuates OGD-Induced Neuronal Cell Death

PRNCs exposed to the OGD condition were then cocultured with HEN6 or fibroblasts in the medium containing VEGF and anti-VEGF. Additional 12 treatment groups (groups G–R) are provided in Figure I in the online-only Data Supplement. On the basis of the apoptosis caspase 3 immunohistochemistry and the MTT assay, we found that PRNCs cocultured with fibroblasts (groups G–L) displayed significant cell death when compared with the singly cultured PRNCs subjected to OGD as described above. However, PRNCs cocultured with HEN6 (groups M–R) exhibited significantly reduced OGD-induced cell death. In addition, VEGF treatments boosted the HEN6

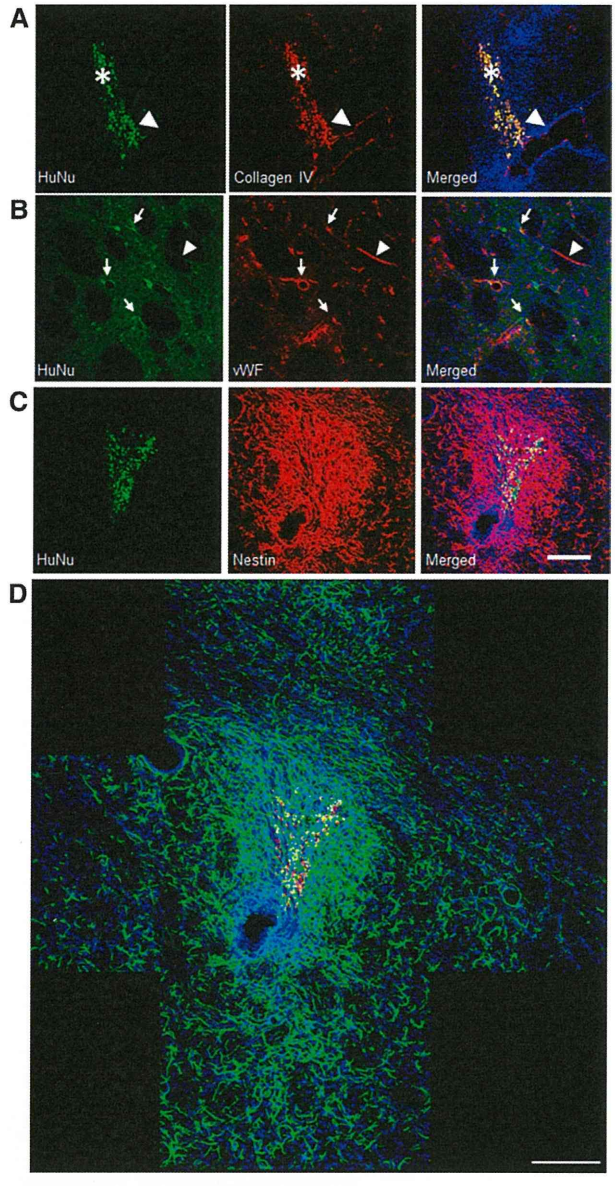

Figure 4. Human cerebral endothelial cells (HEN6) induces endogenous and exogenous vasculogenesis and neurogenesis. HEN6 grafts were labeled with human-specific antigen HuNu (**A–C**; green). The vascular marker collagen IV (**A**; red) revealed labeling of the exogenous transplanted HEN6 (asterisk in **A**) and the endogenous vasculature (arrowhead in **A**). Double positive cells, using the other vascular marker von Willebrand factor (vWF; **B**; red) colabeled with HuNu, correspond to exogenous vasculature (arrow in **B**), whereas vWF-positive cells but negative for HuNu represent endogenous vasculature (arrowhead in **B**). In addition, cells positive for the immature neural marker nestin (**C**; red) and colabeled with the HuNu-positive transplanted HEN6 indicate exogenous neurogenesis, whereas the nestin-positive cells but negative for HuNu represent endogenous neurogenesis. Abundant nestin-positive cells (**D**; green) surrounding the transplants suggest that endogenous neurogenesis within the striatum was enhanced by the HEN6 grafts. Scale bar, 50 μm.

neuroprotective effects that not only blocked the anti-VEGF treatment, but also exacerbated the OGD-induced neurotoxicity. These results were summarized in Figures I and V in the online-only Data Supplement. In the ELISA analysis, VEGF concentrations across all VEGF treatment groups alone and HEN6 alone were comparable and did not differ significantly, except for the combination of HEN6 and VEGF that showed a trend of much higher VEGF upregulation (data not shown). These VEGF-treated groups, as well as the HEN6 alone groups, showed significantly increased levels of VEGF in comparison with no VEGF/no HEN6 coculture and anti–VEGF-treated groups (data not shown).

Discussion

We demonstrated in the present study that transplantation of the human endothelial cell line, HEN6, reduced infarct volume and behavioral deficits accompanied by enhanced endogenous vasculogenesis and neurogenesis and with some grafted cells exhibiting a new microvasculature indicating exogenous vasculogenesis. The mechanism of HEN6 neuroprotective

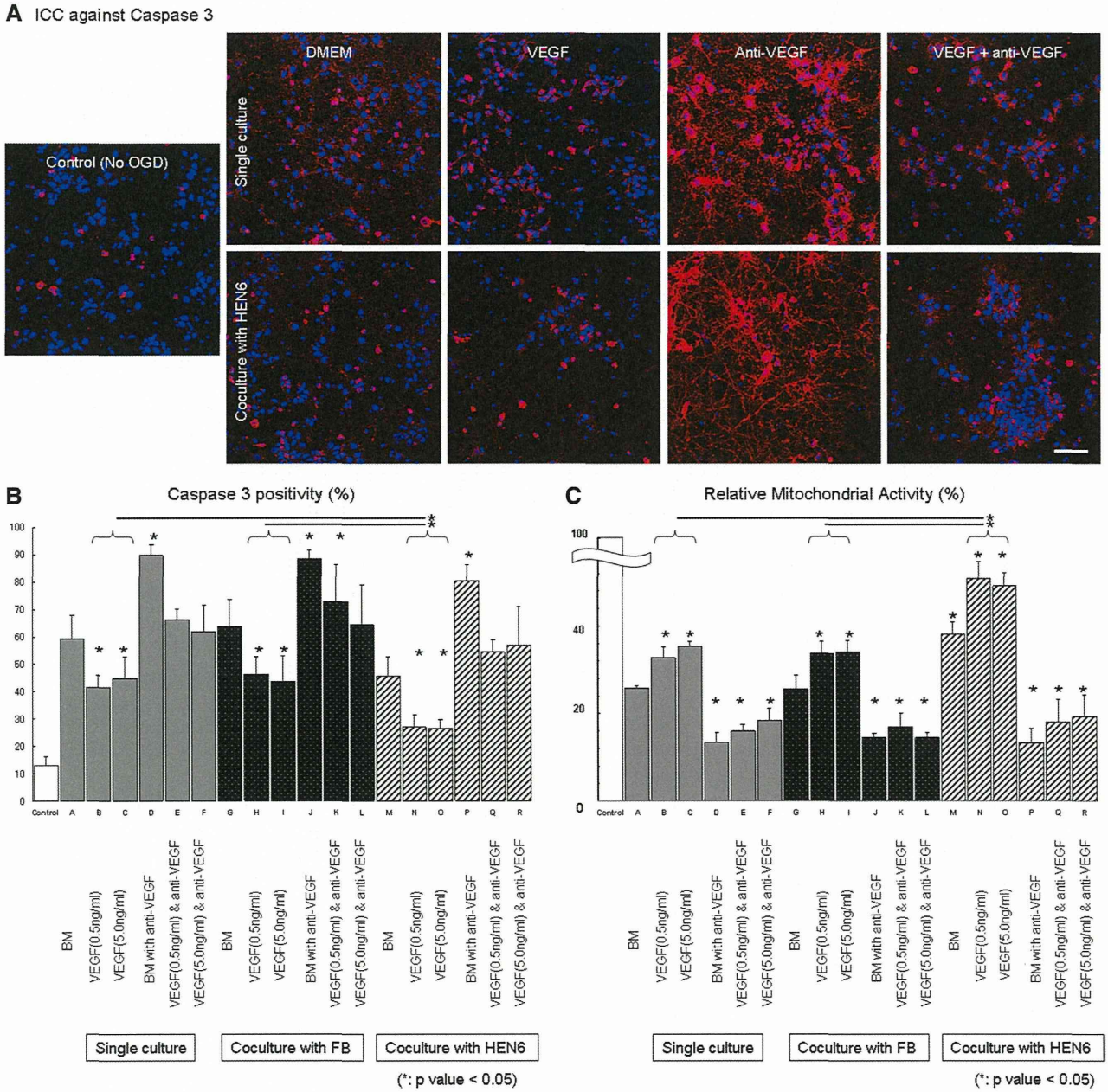

Figure 5. Human cerebral endothelial cells (HEN6) reduces oxygen-glucose deprivation (OGD)–induced cell death in cocultured primary neuronal cells (PRNSCs). Representative caspase 3 immunocytochemical (ICC) images of control (no OGD) vs OGD under single culture of PRNCs or cocultured with HEN6 in the routine DMEM culture condition or supplemented with vascular endothelial growth factor (VEGF), anti-VEGF or combination of both (**A**). In addition, as appropriate coculture control condition, PRNCs were cocultured with fibroblasts (FB; ICC images not shown but comparable with single culture condition). Quantifications of all treatment conditions revealed that OGD produced significant apoptotic cell death (caspase 3; **B**) and impaired the oxidative metabolism (relative mitochondrial activity; **C**), which were blocked by VEGF treatment, and such neuroprotective effects were further enhanced by coculture with HEN6 but not with FB. *P<0.05. Scale bar, 50 μm. BM indicates basal medium.

effects was likely mediated by the VEGF signaling pathway. Altogether, repairing the endothelial component of the neurovascular unit was shown here as a key neuroprotective process for stroke therapy.

Despite the reported functional recovery in transplanted stroke animals and limited clinical trials in patients with stroke,[1–4] a major gap in our knowledge is the mechanism of action underlying cell therapy. We speculated that vascular repair is a vital neuroprotective process in stroke as documented previously.[24,26,35–38] However, it is not clear whether the cell graft-induced neovascularization has endogenous and exogenous components. Furthermore, the correlation between vasculogenesis and neurogenesis in stroke after cell transplantation remains uncertain. Here, we demonstrated that HEN6 transplantation exerted both endogenous and exogenous neovascularization. To this end, we show both collagen IV and vWF as markers of vasculogenesis. In support of delineating endogenous from exogenous vasculogenesis, we observed blood vessels stained with the human-specific antigen marker, HuNu, that colabeled with collagen IV or vWF corresponding to exogenous vasculogenesis (Figure 4). In addition, we detected that juxtaposed to this exogenous vasculogenesis is collagen IV or vWF-stained vessels but without HuNu labeling indicating endogenous vasculogenesis. However, our present data do not distinguish between new vessels and preserved cells after stroke and transplantation. An equally important finding here is that graft-induced vascularization is accompanied by enhanced neurogenesis.[21,38] Similar to our observed exogenous and endogenous vasculogenesis, we found nestin-labeled cells positively or negatively stained with HuNu, suggesting exogenous and endogenous neurogenesis, respectively. Of note, the robust nestin expression enveloping the HuNu-positive cells implies enhanced endogenous neurogenesis. Further characterization of HEN6 graft effects on both angiogenesis and neurogenesis is warranted.

That HEN6 showed VEGF upregulation, and that a trend of improved VEGF elevation detected in the combination group of VEGF and HEN6, both of which blocked by anti-VEGF, suggest that the neuroprotection afforded by HEN6 is regulated by the VEGF pathway. Alternatively, other trophic factors secreted by HEN6 (not examined here) might be contributing additive effects to the exogenous VEGF in producing the neuroprotection against OGD-induced cell death. These therapeutic substances seem to be specific to HEN6 because the fibroblasts coculture did not afford protection against OGD. In addition, the HEN6 cell-to-cell contact with PRNCs, as opposed to the substrate produced by fibroblast-PRNC coculture, could have also mitigated the observed therapeutic benefits. The detection of microvascular morphology in HEN6-grafted stroke animals might have been similarly achieved in the in vitro condition, although likely masked by the short period and incomplete neurovascular unit in the cell culture system. The host microenvironment, in particular the notion of a vasculome in the brain,[39] may also contribute to the fate and function of transplanted cells. These speculative secretory and cell substrate mechanisms warrant further investigations.

HEN6 may display multiple endothelial cell functions, such as enhancing vasculogenesis and fostering the integrity of the blood brain barrier. An important molecule that interacts with endothelial cells is VEGF that could induce vasculogenesis by promoting proliferation and migration of endothelial cells to the site of injury.[40] Furthermore, VEGF is a key factor stimulated within a few hours after cerebral ischemia.[41,42] The present study suggests that a combination of increased VEGF level (as detected in vitro) and enhanced HEN6/host endothelial cell proliferation, migration, and microvasculature-like structure formation within the ischemic brain contributed to the observed therapeutic benefits in this stroke model.

As we translate these findings to the clinic, basic questions on safety and efficacy of the transplant regimen arise. The present intracerebral transplantation targeting the striatal penumbra in the supra-acute stroke stage while effective may not be practical in the clinic. Extending such neurosurgical procedure to a few days after stroke may be more feasible in the clinic. For cell dose, we demonstrated the minimum effective dose of 200K for purified HEN6 transplantation that is comparable with other kinds of cell type.[10,43–47] In view of our findings that VEGF contributed to the therapeutic benefits, combination therapy of VEGF and cell therapy is indicated as described previously.[35,48]

This proof-of-concept study demonstrated efficacy and mechanism of action mediating immortalized cerebral endothelial cell transplantation in stroke. The present 7-day graft maturation period requires long-term assessment of benefit and safety. The present study is focused on the acute therapeutic effects of HEN6 transplantation, warranting the need for determining the chronic effects of cell therapy on angiogenesis and neurogenesis. Although stroke has been widely considered as an acute neurological disease, an equally deleterious secondary cell death ensues after the initial ischemic insult that will require aggressive therapeutic intervention with stable neurostructural and functional benefits over time. Highly regulated immortalized[6,49] or nonimmortalized endothelial progenitor cells[23,24,36,38] have potential cell-based transplant applications in stroke.

Acknowledgments

We express their gratitude to Meaghan Staples, Cyrus Tamboli, Travis Dailey, Chris Metcalf, Diana Hernandez-Ontiveros, Mibel Pabon, and Sandra Acosta for technical assistance during the conduct of the study.

Sources of Funding

Dr Borlongan is supported by James and Esther King Foundation for Biomedical Research Program 1KG01-33966 and National Institutes of Health National Institute of Neurological Disorders and Stroke RO1 1R01NS071956-01.

Disclosures

None.

References

1. Stem Cell Therapies as an Emerging Paradigm in Stroke Participants. Stem cell therapies as an emerging paradigm in stroke (steps): bridging basic and clinical science for cellular and neurogenic factor therapy in treating stroke. *Stroke*. 2009;40:510–515.
2. Borlongan CV, Chopp M, Steinberg GK, Bliss TM, Li Y, Lu M, et al. Potential of stem/progenitor cells in treating stroke: the missing steps in translating cell therapy from laboratory to clinic. *Regen Med*. 2008;3:249–250.
3. Chopp M, Steinberg GK, Kondziolka D, Lu M, Bliss TM, Li Y, et al. Who's in favor of translational cell therapy for stroke: STEPS forward please? *Cell Transplant*. 2009;18:691–693.

4. Kondziolka D, Wechsler L, Goldstein S, Meltzer C, Thulborn KR, Gebel J, et al. Transplantation of cultured human neuronal cells for patients with stroke. *Neurology*. 2000;55:565–569.
5. Jeong SW, Chu K, Jung KH, Kim SU, Kim M, Roh JK. Human neural stem cell transplantation promotes functional recovery in rats with experimental intracerebral hemorrhage. *Stroke*. 2003;34:2258–2263.
6. Lee HJ, Kim KS, Kim EJ, Choi HB, Lee KH, Park IH, et al. Brain transplantation of immortalized human neural stem cells promotes functional recovery in mouse intracerebral hemorrhage stroke model. *Stem Cells*. 2007;25:1204–1212.
7. Borlongan CV, Skinner SJ, Geaney M, Vasconcellos AV, Elliott RB, Emerich DF. CNS grafts of rat choroid plexus protect against cerebral ischemia in adult rats. *Neuroreport*. 2004;15:1543–1547.
8. Wakabayashi K, Nagai A, Sheikh AM, Shiota Y, Narantuya D, Watanabe T, et al. Transplantation of human mesenchymal stem cells promotes functional improvement and increased expression of neurotrophic factors in a rat focal cerebral ischemia model. *J Neurosci Res*. 2010;88:1017–1025.
9. Hayashi J, Takagi Y, Fukuda H, Imazato T, Nishimura M, Fujimoto M, et al. Primate embryonic stem cell-derived neuronal progenitors transplanted into ischemic brain. *J Cereb Blood Flow Metab*. 2006;26:906–914.
10. Kelly S, Bliss TM, Shah AK, Sun GH, Ma M, Foo WC, et al. Transplanted human fetal neural stem cells survive, migrate, and differentiate in ischemic rat cerebral cortex. *Proc Natl Acad Sci USA*. 2004;101:11839–11844.
11. Mimura T, Dezawa M, Kanno H, Yamamoto I. Behavioral and histological evaluation of a focal cerebral infarction rat model transplanted with neurons induced from bone marrow stromal cells. *J Neuropathol Exp Neurol*. 2005;64:1108–1117.
12. Hicks AU, Hewlett K, Windle V, Chernenko G, Ploughman M, Jolkkonen J, et al. Enriched environment enhances transplanted subventricular zone stem cell migration and functional recovery after stroke. *Neuroscience*. 2007;146:31–40.
13. Guzman R, De Los Angeles A, Cheshier S, Choi R, Hoang S, Liauw J, et al. Intracarotid injection of fluorescence activated cell-sorted CD49d-positive neural stem cells improves targeted cell delivery and behavior after stroke in a mouse stroke model. *Stroke*. 2008;39:1300–1306.
14. Minnerup J, Kim JB, Schmidt A, Diederich K, Bauer H, Schilling M, et al. Effects of neural progenitor cells on sensorimotor recovery and endogenous repair mechanisms after photothrombotic stroke. *Stroke*. 2011;42:1757–1763.
15. Sakata H, Niizuma K, Wakai T, Narasimhan P, Maier CM, Chan PH. Neural stem cells genetically modified to overexpress Cu/Zn-superoxide dismutase enhance amelioration of ischemic stroke in mice. *Stroke*. 2012;43:2423–2429.
16. Breier G, Albrecht U, Sterrer S, Risau W. Expression of vascular endothelial growth factor during embryonic angiogenesis and endothelial cell differentiation. *Development*. 1992;114:521–532.
17. Shen Q, Goderie SK, Jin L, Karanth N, Sun Y, Abramova N, et al. Endothelial cells stimulate self-renewal and expand neurogenesis of neural stem cells. *Science*. 2004;304:1338–1340.
18. Strong LH. The early embryonic pattern of internal vascularization of the mammalian cerebral cortex. *J Comp Neurol*. 1964;123:121–138.
19. Shen Q, Wang Y, Kokovay E, Lin G, Chuang SM, Goderie SK, et al. Adult SVZ stem cells lie in a vascular niche: a quantitative analysis of niche cell-cell interactions. *Cell Stem Cell*. 2008;3:289–300.
20. Louissaint A Jr, Rao S, Leventhal C, Goldman SA. Coordinated interaction of neurogenesis and angiogenesis in the adult songbird brain. *Neuron*. 2002;34:945–960.
21. Palmer TD, Willhoite AR, Gage FH. Vascular niche for adult hippocampal neurogenesis. *J Comp Neurol*. 2000;425:479–494.
22. Kiel MJ, Yilmaz OH, Iwashita T, Yilmaz OH, Terhorst C, Morrison SJ. SLAM family receptors distinguish hematopoietic stem and progenitor cells and reveal endothelial niches for stem cells. *Cell*. 2005;121:1109–1121.
23. Asahara T, Murohara T, Sullivan A, Silver M, van der Zee R, Li T, et al. Isolation of putative progenitor endothelial cells for angiogenesis. *Science*. 1997;275:964–967.
24. Urbich C, Dimmeler S. Endothelial progenitor cells: characterization and role in vascular biology. *Circ Res*. 2004;95:343–353.
25. Moubarik C, Guillet B, Youssef B, Codaccioni JL, Piercecchi MD, Sabatier F, et al. Transplanted late outgrowth endothelial progenitor cells as cell therapy product for stroke. *Stem Cell Rev*. 2011;7:208–220.
26. Oyamada N, Itoh H, Sone M, Yamahara K, Miyashita K, Park K, et al. Transplantation of vascular cells derived from human embryonic stem cells contributes to vascular regeneration after stroke in mice. *J Transl Med*. 2008;6:54.
27. Borlongan CV, Hadman M, Sanberg CD, Sanberg PR. Central nervous system entry of peripherally injected umbilical cord blood cells is not required for neuroprotection in stroke. *Stroke*. 2004;35:2385–2389.
28. Borlongan CV, Lind JG, Dillon-Carter O, Yu G, Hadman M, Cheng C, et al. Bone marrow grafts restore cerebral blood flow and blood brain barrier in stroke rats. *Brain Res*. 2004;1010:108–116.
29. Borlongan CV, Lind JG, Dillon-Carter O, Yu G, Hadman M, Cheng C, et al. Intracerebral xenografts of mouse bone marrow cells in adult rats facilitate restoration of cerebral blood flow and blood-brain barrier. *Brain Res*. 2004;1009:26–33.
30. Borlongan CV, Skinner SJ, Geaney M, Vasconcellos AV, Elliott RB, Emerich DF. Intracerebral transplantation of porcine choroid plexus provides structural and functional neuroprotection in a rodent model of stroke. *Stroke*. 2004;35:2206–2210.
31. Parxinos G, Watson C. *The Rat Brain in Stereotaxic Coordinates*. New York: Academic Press; 2005.
32. Matsukawa N, Yasuhara T, Hara K, Xu L, Maki M, Yu G, et al. Therapeutic targets and limits of minocycline neuroprotection in experimental ischemic stroke. *BMC Neurosci*. 2009;10:126.
33. Borlongan CV, Kaneko Y, Maki M, Yu SJ, Ali M, Allickson JG, et al. Menstrual blood cells display stem cell-like phenotypic markers and exert neuroprotection following transplantation in experimental stroke. *Stem Cells Dev*. 2010;19:439–452.
34. Bell E, Cao X, Moibi JA, Greene SR, Young R, Trucco M, et al. Rapamycin has a deleterious effect on MIN-6 cells and rat and human islets. *Diabetes*. 2003;52:2731–2739.
35. Harms KM, Li L, Cunningham LA. Murine neural stem/progenitor cells protect neurons against ischemia by HIF-1alpha-regulated VEGF signaling. *PLoS One*. 2010;5:e9767.
36. Nakagomi N, Nakagomi T, Kubo S, Nakano-Doi A, Saino O, Takata M, et al. Endothelial cells support survival, proliferation, and neuronal differentiation of transplanted adult ischemia-induced neural stem/progenitor cells after cerebral infarction. *Stem Cells*. 2009;27:2185–2195.
37. Shimotake J, Derugin N, Wendland M, Vexler ZS, Ferriero DM. Vascular endothelial growth factor receptor-2 inhibition promotes cell death and limits endothelial cell proliferation in a neonatal rodent model of stroke. *Stroke*. 2010;41:343–349.
38. Taguchi A, Soma T, Tanaka H, Kanda T, Nishimura H, Yoshikawa H, et al. Administration of CD34+ cells after stroke enhances neurogenesis via angiogenesis in a mouse model. *J Clin Invest*. 2004;114:330–338.
39. Guo S, Zhou Y, Xing C, Lok J, Som AT, Ning M, et al. The vasculome of the mouse brain. *PLoS One*. 2012;7:e52665.
40. Senger DR, Galli SJ, Dvorak AM, Perruzzi CA, Harvey VS, Dvorak HF. Tumor cells secrete a vascular permeability factor that promotes accumulation of ascites fluid. *Science*. 1983;219:983–985.
41. Jin K, Mao XO, Greenberg DA. Vascular endothelial growth factor stimulates neurite outgrowth from cerebral cortical neurons via Rho kinase signaling. *J Neurobiol*. 2006;66:236–242.
42. Plate KH, Beck H, Danner S, Allegrini PR, Wiessner C. Cell type specific upregulation of vascular endothelial growth factor in an MCA-occlusion model of cerebral infarct. *J Neuropathol Exp Neurol*. 1999;58:654–666.
43. Chu K, Kim M, Park KI, Jeong SW, Park HK, Jung KH, et al. Human neural stem cells improve sensorimotor deficits in the adult rat brain with experimental focal ischemia. *Brain Res*. 2004;1016:145–153.
44. Saporta S, Borlongan CV, Sanberg PR. Neural transplantation of human neuroteratocarcinoma (hNT) neurons into ischemic rats. A quantitative dose-response analysis of cell survival and behavioral recovery. *Neuroscience*. 1999;91:519–525.
45. Borlongan CV, Tajima Y, Trojanowski JQ, Lee VM, Sanberg PR. Cerebral ischemia and CNS transplantation: differential effects of grafted fetal rat striatal cells and human neurons derived from a clonal cell line. *Neuroreport*. 1998;9:3703–3709.
46. Grabowski M, Johansson BB, Brundin P. Survival of fetal neocortical grafts implanted in brain infarcts of adult rats: the influence of postlesion time and age of donor tissue. *Exp Neurol*. 1994;127:126–136.
47. Darsalia V, Allison SJ, Cusulin C, Monni E, Kuzdas D, Kallur T, et al. Cell number and timing of transplantation determine survival of human neural stem cell grafts in stroke-damaged rat brain. *J Cereb Blood Flow Metab*. 2011;31:235–242.
48. Maurer MH, Thomas C, Bürgers HF, Kuschinsky W. Transplantation of adult neural progenitor cells transfected with vascular endothelial growth factor rescues grafted cells in the rat brain. *Int J Biol Sci*. 2008;4:1–7.
49. Aboody KS, Bush RA, Garcia E, Metz MZ, Najbauer J, Justus KA, et al. Development of a tumor-selective approach to treat metastatic cancer. *PLoS One*. 2006;1:e23.

Ischemic Stroke Brain Sends Indirect Cell Death Signals to the Heart

Hiroto Ishikawa, MD, PhD; Naoki Tajiri, PT, PhD; Julie Vasconcellos, BS; Yuji Kaneko, PhD; Osamu Mimura, MD, PhD; Mari Dezawa, MD, PhD; Cesar V. Borlongan, PhD

Background and Purpose—Ischemic stroke is a leading cause of mortality and morbidity in the world and may be associated with cardiac myocyte vulnerability. However, it remains uncertain how an ischemic brain contributes to cardiac alternations. Here, we used experimental stroke models to reveal the pathological effects of the ischemic brain on the heart.

Methods—For the in vitro study, primary rat neuronal cells were subjected to 90-minute oxygen–glucose deprivation (OGD). Two hours after OGD, the supernatant was collected and cryopreserved until further biological assays. Primary rat cardiac myocytes were exposed to ischemic–reperfusion injury and subsequently to the supernatant derived from either the OGD or non–OGD-exposed primary rat neuronal cells for 2, 6, 24, or 48 hours. Thereafter, we measured cell viability and mitochondrial activity in rat cardiac myocytes. For the in vivo study, we subjected adult rats to transient middle cerebral artery occlusion, and their brains and hearts were harvested for immunohistochemical analyses at 3 months later.

Results—The supernatant from the OGD, but not the non–OGD-exposed primary rat neuronal cells, caused significant reduction in cell viability and mitochondrial activity in rat cardiac myocytes. Ischemic stroke animals displayed phenotypic expression of necrosis, apoptosis, and autophagy in their hearts, which paralleled the detection of these same cell death markers in their brains.

Conclusions—Ischemic stroke was accompanied by cardiac myocyte death, indicating a close pathological link between brain and heart. These results suggest a vigilant assessment of the heart condition in stroke patients, likely requiring the need to treat systemic cardiac symptoms after an ischemic brain episode. **(*Stroke*. 2013;44:3175-3182.)**

Key Words: apoptosis ■ autophagy ■ brain ischemia ■ myocytes, cardiac ■ necrosis

Ischemic heart and cerebrovascular disease are the first and second leading causes of death in the world. The United States spends $206.8 billion for cardiac disease and $53.9 billion for ischemic stroke, including expenses for healthcare services, medications, and loss of productivity.[1,2] The risk factors of cardiovascular or cerebrovascular diseases involve environmental and genetic entities, most notably high blood cholesterol levels, high blood pressure, diabetes mellitus, obesity, and history of cardiovascular diseases.[3–5]

In the clinic, most deaths following ischemic stroke are a direct result of neurological damage. Second to neurologically linked fatalities are deaths caused by cardiac failure.[6,7] Of note, 2% to 6% of deaths are of cardiac origins in the 3 months following ischemic stroke.[7,8] Although this percentage of cardiac cell death declines after the early stage, data show that those who have ischemic stroke are more likely to present with cardiac death than age-matched nonstroke victims, with the former exhibiting abnormal rhythms in ECG, as well as large changes in cardiac enzyme and plasma catecholamines.[9] Cardiac enzymes are most closely associated with elevated troponin and creatine phosphokinase levels, which become evident when cardiac cells are under stress and dying.[10] Increased catecholamine levels are associated with high blood pressure and tachycardia and are present also during stress.[11]

For years, the correlation between cerebrovascular incidents had been ascribed primarily to overlapping risk factors. However, damage to the insular cortex has been shown to produce a high incidence of cardiac death compared with other brain regions, in that up to 88% of patients with insular cortical stroke present with cardiac symptoms in the following weeks after stroke.[12] The role of the insular cortex in sympathetic and parasympathetic nervous system control has been implicated in the observed cardiac alterations.[13] Cardiac autonomic tone is controlled by the insular cortex, and with the loss of this regulatory function after stroke, cardiac compromise is more likely to ensue.[13] Disagreement remains on whether a specific region of the insular cortex or as a whole differentially causes cardiac myocyte death. Indeed, insular cortex damage is rarely seen without injury to other structures in the brain when middle cerebral artery occlusion (MCAo) is induced. Therefore,

Received April 5, 2013; final revision received July 6, 2013; accepted July 23, 2013.

From the Department of Neurosurgery and Brain Repair, University of South Florida College of Medicine, Tampa, FL (H.I., N.T., J.V., Y.K., C.V.B.); Department of Ophthalmology, Hyogo College of Medicine, Nishinomiya, Japan (H.I., O.M.); and Department of Stem Cell Biology and Histology and Department of Anatomy and Anthropology, Tohoku University Graduate School of Medicine, Sendai, Japan (M.D.).

Correspondence to Cesar V. Borlongan, PhD, Department of Neurosurgery and Brain Repair, University of South Florida, 12901 Bruce B. Downs Blvd MDC78, Tampa, FL 33612. E-mail cborlong@health.usf.edu

Stroke **is available at http://stroke.ahajournals.org** **DOI: 10.1161/STROKEAHA.113.001714**

the direct involvement of the insular cortex in cardiovascular disorders following stroke is still not well established.

In the present study, we explored the relationship between neuronal cell death and cardiac myocyte compromise using both in vitro and in vivo stroke models. For the in vitro study, we used the oxygen–glucose deprivation (OGD) condition in primary rat neuronal cells (PRNCs) and used the supernatant to explore cellular changes in rat cardiac myocytes (RCMs) following ischemic–reperfusion (I/R) injury. For the in vivo study, we induced transient MCAo in adult rats and performed immunohistochemical analyses on the brains and hearts of stroke rats to reveal different cell death markers. We hypothesized that the ischemic brain compromises cardiac myocytes through secretion of cell death factors.

Material and Methods

In Vitro Study

Cell Culture

PRNCs were obtained from BrainBits. As per the manufacturer's protocol, cells (4×10^4 cells/well) were suspended in 200 μL supplemented neurobasal medium containing 2 mmol/L L-glutamine and 2% B27 in the absence of antibiotics and grown in Poly-L-Lysine-coated 96-well (BD Biosciences) at 37°C in humidified atmosphere containing 5% carbon dioxide. PRNCs were grown until reaching ≈70% cell confluence. We immunocytochemically determined that PRNCs expressed the vesicular glutamate transporter-1. Thereafter, PRNCs were subjected to OGD condition as described below.

RCMs were obtained from Lonza. As per the manufacturer's protocol, cells (1.5×10^5 cells/well) were suspended in 200 μL supplemented rat cardiac myocyte basal medium (Lonza) containing rat cardiac growth medium SingleQuots and incubated for 4 hours in nitrocellulose-coated 96-well at 37°C in humidified atmosphere containing 5% carbon dioxide. At day 1 in vitro (DIV1), 80% of medium was removed from the cells and treated with prewarmed rat cardiac myocyte basal medium containing 200 μmol/L BrdU for 4 hours. At DIV3, 50% of the medium was removed from the cells and changed to a fresh rat cardiac myocyte basal medium containing 200 μmol/L BrdU. Thereafter, at DIV5, RCMS were subjected to further experiments as described below.

OGD in PRNCs

At DIV5, PRNCs were subjected to 90 minutes OGD condition as described previously.[14] Briefly, the neuronal cells were initially exposed to OGD medium (116 mmol/L NaCl, 5.4 mmol/L KCl, 0.8 mmol/L $MgSO_4$, 1 mmol/L NaH_2PO_4, 26.2 mmol/L $NaHCO_3$, 0.01 mmol/L glycine, 1.8 mmol/L $CaCl_2$, pH 7.4), placed in an anaerobic chamber (PlasLabs) containing 95% nitrogen and 5% carbon dioxide for 15 minutes at 37°C, and finally the chamber was sealed and incubated for 90 minutes at 37°C (hypoxic-ischemic condition). After the hypoxic-ischemic condition, the culture was reintroduced to the normoxic condition containing 5 mmol/L glucose for 2 hours resembling a reperfusion. Thereafter, the supernatant was collected from the culture and subjected to the following experiments described below.

I/R Injury in RCMs

At DIV5, RCMs were subjected to I/R injury using OGD condition. After I/R injury, RCMs were incubated with DMEM or the supernatant from PRNCs in normoxic condition. To determine the exposure period that was most toxic, we preset the reperfusion at different time points as follows: Group A: 2 hours incubation with DMEM without I/R injury as a control; Group B: 2 hours reperfusion with DMEM; Group C: 6 hours reperfusion with DMEM; Group D: 24 hours reperfusion with DMEM; Group E: 48 hours reperfusion with DMEM; Group F: 2 hours incubation with the supernatant from PRNCs without I/R injury; Group G: 2 hours reperfusion with the supernatant from PRNCs; Group H: 6 hours reperfusion with the supernatant; Group I: 24 hours reperfusion with the supernatant; and Group J: 48 hours reperfusion with the supernatant, which are summarized in the Table. Thereafter, RCMs were subjected to further analyses.

Immunocytochemistry

To confirm that the OGD condition produced neuronal death in PRNCs, immunohistochemistry was performed. After OGD condition, PRNCs were rinsed twice in PBS and fixed in 4% paraformaldehyde fixative for 5 minutes at room temperature. After the fixation, cells were rinsed in PBS and PBS containing Tween-20 (ab 64247; abcam) (PBST) twice each. Then they were blocked by 5% goat serum (50062Z; Invitrogen) for 30 minutes at room temperature. They were incubated with first antibodies; an anti–tumor necrosis factor (TNF)-α antibody (mouse monoclonal [ab1793]; abcam) for necrosis, anti–active Caspase 3 antibody (rabbit polyclonal [ab13847]; abcam) for apoptosis, anti–Fas Ligand antibody (rabbit polyclonal [ab15285]; abcam) for apoptosis, and anti-MAP1LC3A antibody (rabbit polyclonal [ab64123]; abcam) for autophagy, with 5% serum and 0.2% triton X-100 (Fischer Scientific, Pittsburgh, PA) for 1 hour at room temperature. After primary antibody incubation, they were rinsed twice in PBST again. Next, they were incubated in secondary antibodies; goat anti–mouse IgG Alexa Fluor 488 conjugate (Invitrogen) and goat anti–rabbit IgG Alexa Fluor 594 conjugate (Invitrogen) for 1 hour at room temperature. After incubation with secondary antibodies, they were rinsed in PBST and PBS twice each. Thereafter, they

Table. Summary of Experimental Groups and Immunohistochemical Results of Cell Death Markers in the In Vitro Study

Groups	A	B	C	D	E	F	G	H	I	J
Injury	No	I/R	I/R	I/R	I/R	No	I/R	I/R	I/R	I/R
Medium	DMEM	DMEM	DMEM	DMEM	DMEM	Supernatant from PRNCs	Supernatant from PRNCs	Supernatant from PRNCs	Supernatant from PRNCs	Supernatant from PRNCs
Reperfusion time (h)	2	2	6	24	48	2	2	6	24	48
TNF-α	11.0±7.0%	27.5±13.5%	35.8±22.6%	32.8±14.0%	45.2±19.3%	15.3±14.2%	36.4±19.9%	38.6±24.9%	51.4±31.7%	60.2±30.1%
Caspase 3	27.9±12.3%	32.6±17.1%	53.1±11.4%	59.8±16.7%	73.5±12.0%	27.5±11.7%	34.7±10.1%	69.8±10.4%	71.3±8.4%	89.4±4.6%
Fas Ligand	35.4±9.0%	44.3±17.6%	61.0±12.9%	59.6±15.1%	76.1±16.5%	42.4±19.9%	55.6±18.7%	59.4±15.6%	73.0±17.6%	87.2±7.7%
MAP1LC3A	30.7±8.7%	27.2±8.3%	51.7±15.2%	86.5±11.2%	82.9±10.4%	42.0±18.6%	59.9±31.6%	73.3±13.4%	85.5±12.4%	95.2±3.3%

Rat cardiac myocytes were cultured for 5 days and then subjected to ischemic–reperfusion (I/R) injury. Group A: 2 hours incubation with DMEM without I/R injury as a control, Group B: 2 hours reperfusion with DMEM, Group C: 6 hours reperfusion with DMEM, Group D: 24 hours reperfusion with DMEM, Group E: 48 hours reperfusion with DMEM, Group F: 2 hours incubation with the supernatant from primary rat neuronal cells (PRNCs) without I/R injury, Group G: 2 hours reperfusion with the supernatant from PRNCs, Group H: 6 hours reperfusion with the supernatant, Group I: 24 hours reperfusion with the supernatant, and Group J: 48 hours reperfusion with the supernatant. TNF-α indicates tumor necrosis factor-α.

were incubated with Hoechst 33342 (Sigma) for 10 minutes at room temperature for nucleus staining and rinsed twice in PBS.

Next, to reveal the toxicity of the supernatant harvested from PRNCs on RCMs, RCMs were subjected to I/R injury (as described above), then subsequently exposed to the supernatant from OGD- or non–OGD-exposed PRNCs and processed for immunocytochemical analyses of cell death.

Cell Viability Assay

Measurement of RCMs viability was performed using fluorescent live/dead cell assay.[15] A 2-color fluorescence cell viability assay was performed using calcein-AM (Invitrogen) that revealed an intense uniform green fluorescence in live cells and ethidium homodimer (EthD-1, Invitrogen) characterized by red fluorescence bound to the nuclei of damaged cells. Following IR injury, the cells were incubated with 2 μmol/L calcein-AM and 4 μmol/L EthD-1 for 45 minutes at room temperature in darkness. After washing with PBS, the green fluorescence of the live cells was measured by the Gemini EX florescence plate reader (Molecular Device), with excitation at 485 nm and emission at 538 nm. To calibrate the cell viability precisely, the values were standardized from florescence intensity.

Mitochondrial Activity Assay

Changes in 3-(4, 5-dimethyl-2-thiazoyl)-2, 5-diphenyltetrazolium bromide (MTT) as revealed by cellular dehydrogenases has been used as a measure of mitochondrial activity. MTT assay was performed according to the manufacturer's protocol (Roche) as previously described.[16] After I/R injury, the RCMs were incubated with 0.5 mg/mL MTT 37°C and 5% CO_2 and incubated with lysis buffer overnight in a humidified atmosphere at 37°C and 5% CO_2. The optical density of solubilized purple formazan was measured at 570 nm on a Synergy HT plate reader (Bio-Tex).

In Vivo Study

Stroke Surgery

Stroke surgery was performed using the transient MCAo model as previously described.[17,18] Animals were anesthetized with 1% to 2% isoflurane in nitrous oxide/oxygen (69%/30%) using a face mask. Body temperature was maintained at 37°C ±0.3°C during the surgical procedures. A midline skin incision was made in the neck with subsequent exploration of the right common carotid artery, the external carotid artery, and internal carotid artery. A 4-0 monofilament nylon suture (27–28 mm) was advanced from the common carotid artery bifurcation until it blocked the origin of the MCA. Animals were allowed to recover from anesthesia during MCAo. After 60 minutes of transient MCAo, animals were reanesthetized and reperfused by withdrawal of the nylon thread. The animals were then closed and allowed to recover from anesthesia. We have previously standardized the MCAo model, with stroke animals showing ≥80% reduction in regional cerebral blood flow during the occlusion period as determined by laser Doppler (Perimed). To further ensure similar degree of stroke insults, physiological parameters including Pao_2, $PaCO_2$, and plasma pH measurements were monitored, and we found no significant differences in our stroke animals. We initially used 10 rats for the stroke surgery and subsequently included 8 rats that reached the criterion of 80% cerebral blood flow reduction during occlusion. Age-matched animals that were exposed to sham surgery served as controls. However, during the initial conduct of analyses, only trace levels or nondetectable signals of all cell death markers were obtained from these sham animals, thus subsequent analyses (reported here) focused on stroke animals.

Histology and Immunohistochemistry

Rats were deeply anesthetized and perfused transcardially with 4% paraformaldehyde fixative at 3 months after MCAo. Brains and hearts were harvested and postfixed in the same fixative for 24 hours, followed by 30% sucrose in PBS for 1 week. Frozen sections were then cut at 30 μm in a cryostat and stored at −20°C. To demonstrate cell death, immunohistochemical investigations were performed. Frozen sections were incubated overnight at 4°C with first antibodies tested for in vitro study. After rinsing 3 times in PBS, sections were incubated for 2 hours at room temperature in the same secondary antibodies as noted above for immunocytochemistry and with Hoechst33342 (Sigma) as counterstain. The sections were washed again 3 times in PBS and mounted on glass slides using mounting medium. Control studies included exclusion of primary antibody substituted with 10% goat serum in PBS. No immunoreactivity was observed in these controls.

Evaluation of Immunostained Cells

To evaluate the number of immunopositive cells, we semiquantitatively defined cells as follows: no positive cells (no cells/1 visual filed): (−), low (1–3 cells): (+), medium (4–9 cells): (++), high (>10 cells): (+++).

Statistical Analysis

Analysis of variance and post hoc *t* test were used for statistical analyses. All data were presented as mean±SEM. In all analyses, $P<0.05$ was considered statistically significant.

Results

PRNCs and RCMs Are Vulnerable to Cell Death After I/R Injury

PRNCs after OGD displayed significant cell death. Necrotic cells (TNF-α–positive cells) were widespread under OGD (20.3±9.0%), but limited under normal condition (8.2±4.7%) ($P<0.05$). Apoptotic Caspase 3-positive cells were rampant in PRNCs under OGD (78.4±19.1%) and higher than PRNCs in normal condition (43.1±9.8%) ($P<0.05$). Fas Ligand–positive apoptotic cells were markedly increased in OGD (77.7±7.0%) compared with normal condition (14.6±4.9%) ($P<0.01$). In addition, autophagic MAP1L3CA-positive cells were significantly higher in OGD (86.3±6.4%) than normal condition (39.4±8.3%) ($P<0.01$) (Figure 1).

In immunocytochemical analyses of RCMs, all cell death markers were significantly increased after I/R injury compared with normal condition (summarized in Table). Analyses of necrosis revealed TNF-α immunoreactivity was increased and reached over 40% at 48 hours after I/R injury. Analyses of apoptosis showed the number of cells expressing Caspase 3 and Fas Ligand immunoreactivity were increased time dependently and reached over 70% at 48 hours after I/R injury. In the analyses of autophagy-related cell death, the number of cells with MAP1LC3A immunoreactivity reached over 80% and peaked at 24 hours after I/R injury (Figure 2).

Supernatant From PRNCs Is Toxic to RCMs

Next, we used the supernatant from OGD-exposed PRNCs as a medium in RCMs culture after I/R injury to examine whether the supernatant produced an exacerbating toxic effect on the cardiac myocytes. In immunocytochemical analyses of RCMs with the OGD supernatant, all cell death markers were detected (summarized in Table). Analyses of necrosis revealed TNF-α immunoreactivity in the OGD supernatant groups (Group I and J) was significantly higher at 24 and 48 hours after I/R injury compared with the non-OGD groups (Group D and E) ($P<0.05$), with >60% necrotic cells detected

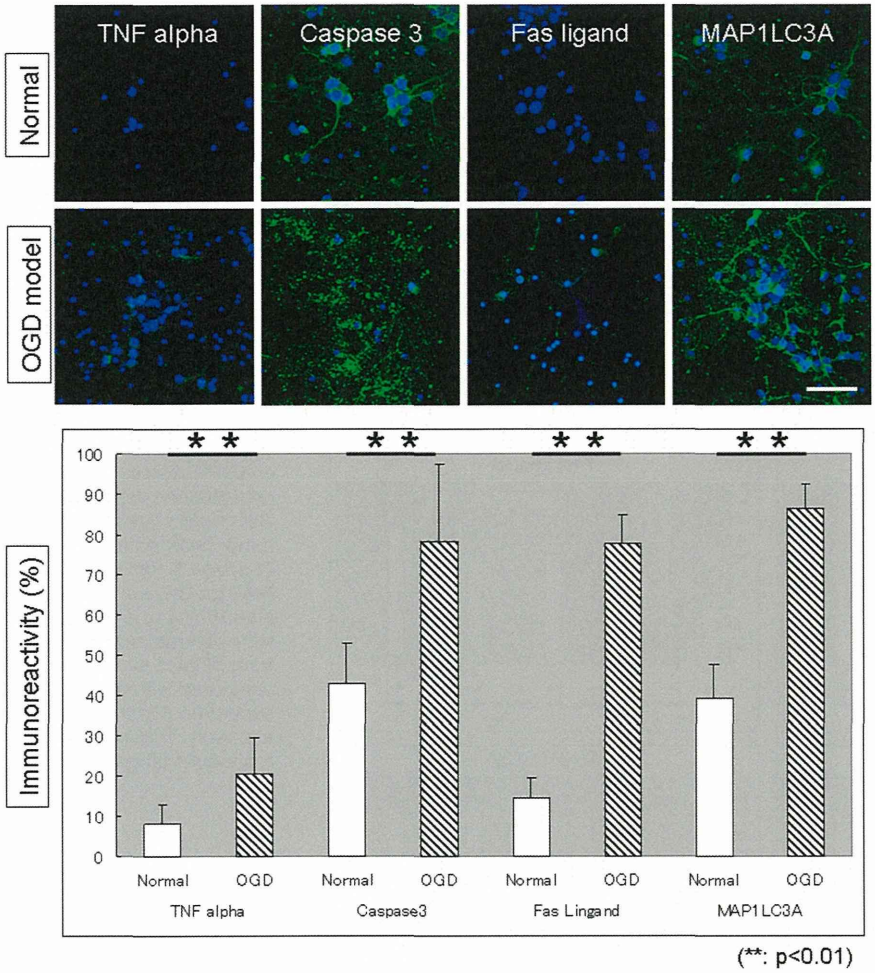

Figure 1. Immunocytochemical analyses of primary rat neuronal cells after oxygen–glucose deprivation (OGD) condition. Cell death markers of necrosis, apoptosis, autophagy were elevated after OGD as evidenced by significantly increments in tumor necrosis factor-α (TNF-α), Caspase 3, Fas Ligand, and MAP1LC3A labeled cells compared with normal condition. Scale bar represents 50 μm.

at 48 hours after I/R injury. Analyses of apoptosis demonstrated time-dependent increments in Caspase 3 and Fas Ligand immunoreactivity. Significant increments in Caspase 3 immunoreactivity started as early as 6 hours after I/R injury, whereas Fas Ligand exhibited significant increments not until 24 hours after I/R injury ($P<0.05$). Both Caspase 3 and Fas Ligand in the OGD supernatant groups reached over 80% immunoreactivity at 48 hours after I/R injury. In the analyses of autophagy-related cell death, significant elevation of MAP1LC3A immunoreactivity was detected as early as 2 hours after I/R injury ($P<0.05$) and reached over 90% immunoreactivity at 48 hours after I/R injury (Figure 2).

In analyzing cell viability and mitochondrial activity in RCMs, I/R injury alone without the supernatant from OGD-exposed PRNCs (DMEM treatment group) did not lead to cardiac myocyte cell death, even up to 48 hours after I/R injury. With the addition of the supernatant from OGD-exposed PRNCs, calcein assay showed that RCM viability significantly decreased at 24 hours after I/R injury compared with normoxic condition (control) or versus non-OGD (DMEM) treated groups ($P<0.01$). In the MTT assay, the relative mitochondrial reductase activity of RCMs was also significantly reduced with the additional of the supernatant from OGD-exposed PRNCs at 48 hours after I/R injury ($P<0.05$) (Figure 3).

Both Brain and Heart in Chronic Ischemic Stroke Rats Exhibit Cell Death

Immunohistochemical results revealed cell death in the ischemic stroke brain and heart. In the brain analyses, all cell death markers were positive in ipsilateral side; TNF-α–positive and Fas Ligand–positive cells were mostly found in the ipsilateral side, while Caspase 3 and MAP1LC3A were positive in both hemispheres, the contralateral side immunoreactivity was less intense than ipsilateral side (Figure 4). In the heart analyses, all cell death markers were detected in cardiac myocytes; low number of TNF-α–positive and Fas Ligand–positive cells (+), moderate number of Caspase 3-positive cells (++), and high number of MAP1LC3A-positive cells (+++) were detected in the heart after ischemic stroke. The immunoreactivity of the same cell death markers in brains and hearts from sham animals was less intense than those from stroke animals (Figure 4).

Discussion

In the present study, we explored whether ischemic stroke conferred cell death signals to the heart. The in vitro study showed that the supernatant from ischemic (ie, OGD exposed) PRNCs rendered toxic effects on RCMs. Similarly, the in vivo study showed that ischemic stroke animals exhibited RCM cell death. Altogether these results suggest a close pathological link between ischemic stroke and cardiac arrest.

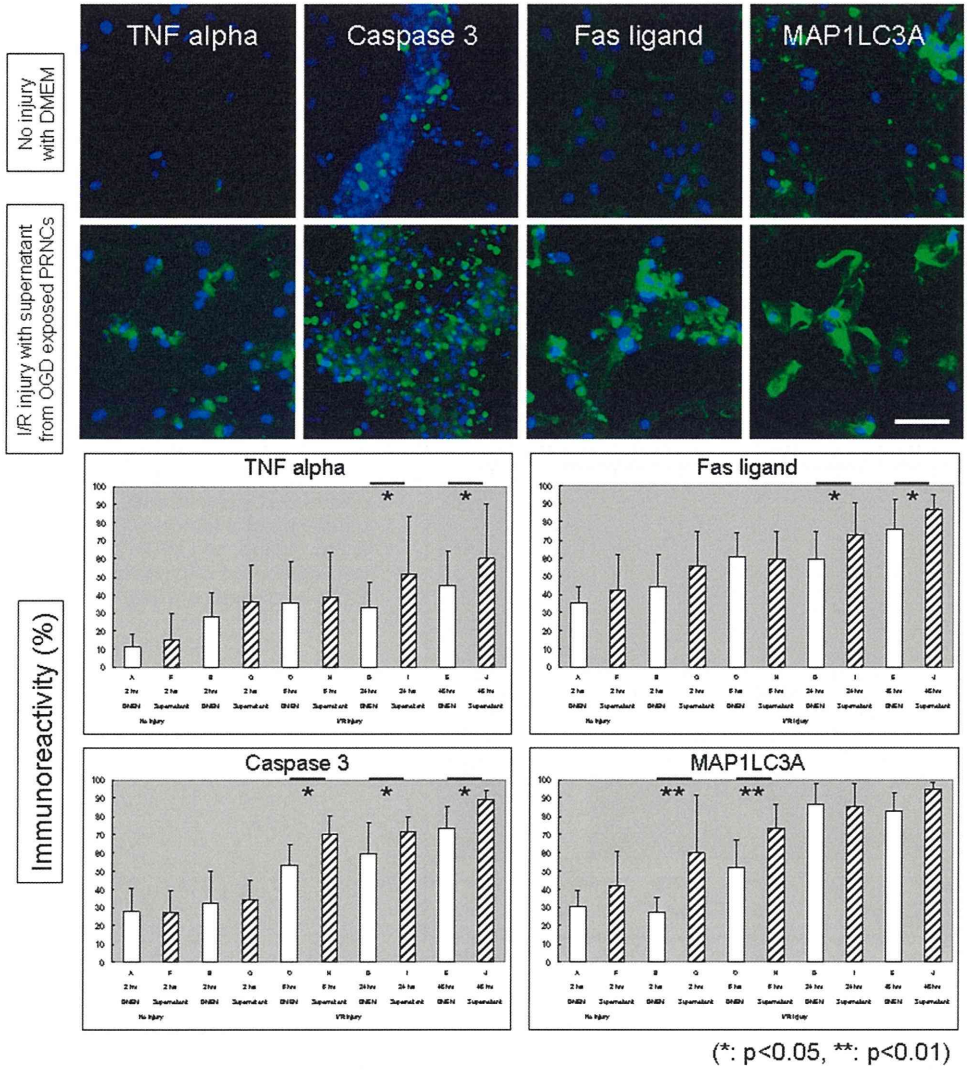

Figure 2. Immunocytochemical analyses of rat cardiac myocytes (RCMs) after ischemic–reperfusion (I/R) injury and treatment with supernatant harvested from primary rat neuronal cells (PRNCs) exposed to oxygen–glucose deprivation (OGD). Cell death markers, including tumor necrosis factor-α (TNF-α), Caspase 3, Fas Ligand, and MAP1LC3A, were elevated after I/R injury and treatment with supernatant harvested from PRNCs exposed to OGD compared with the addition of supernatant from non–OGD-exposed PRNCs. Scale bar represents 50 μm.

Heart failure and ischemic brain stroke are major causes of mortality and disability around the world.[19] Sometimes, the failure of these 2 organs occurs simultaneously, resulting in a more severe condition. The present study focused on cardiac myocyte death following ischemic stroke, using experimental in vitro and in vivo stroke models. Cardiac arrest leading to brain damage has been previously reported.[8,20] Here, we show that ischemic stroke could also lead to cardiac alterations.

How does the ischemic stroke disrupt heart function? A normal, nonpathogenic heart autonomously beats while the brain controls heart rate via adrenergic pathways affected by exercises and emotions.[21] Previous clinical studies have shown that the damaged brain, as a consequence of ischemic stroke, is not able to control the heart rhythms suggesting that the heart compromise may be a direct result of ischemic stroke.[8,12] The insular cortex in the brain is most closely linked to the heart rhythm control,[22] as documented in laboratory and clinical studies,[23–25] indicating a close interaction between heart alterations and insular cortex damage following ischemic stroke. Interestingly, an ischemic event increases inflammation in atherosclerotic plaques and extramedullary monocytopoiesis via progenitor cells released from the bone marrow stromal niche, resulting in plaque rupture.[26] However, heart compromise following ischemic stroke unrelated to insular cortical damage has also been reported,[21] supporting the notion of an indirect control of heart alterations by the ischemic brain. Accordingly, a key rationale in the present study is to explore this indirect cell death pathway between the brain and heart.

An unexpected finding of this study is that the direct I/R injury to the RCMs (without OGD supernatant from PRNCs, only DMEM; Figure 3) actually did not cause cardiac myocyte death (see calcein and MTT assays), which might reflect a compensatory protective mechanism during the acute stage of injury (0–48 hours). The addition of OGD supernatant was shown here to trigger the massive cell death to the heart, suggesting that the indirect pathway of ischemic stroke regulating cardiac cell death plays an important role in cardiac failure which until now has not been fully recognized. Other potentially parallel pathways linking stroke and cardiac cell death also need to be considered including systemic inflammatory responses,[27,28] neuroendocrine-mediated myocardial suppression,[7,29] and changes in circulating endothelial progenitor cells.[30]

Immunocytochemical analyses of PRNCs after OGD and RCMs after I/R injury showed that all cell death markers were

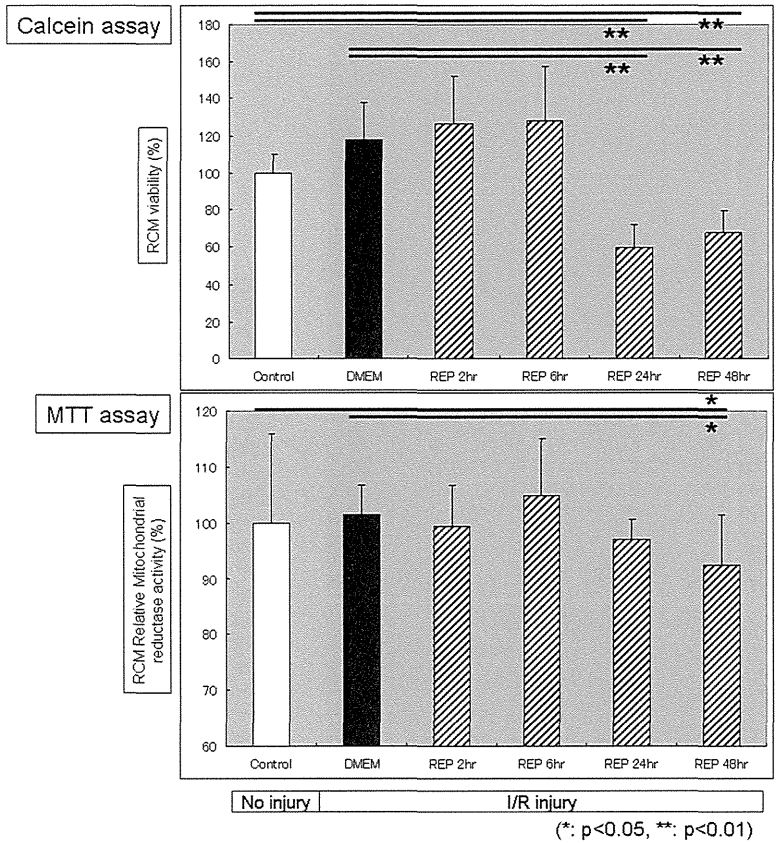

Figure 3. *Cell viability and mitochondrial activity* in rat cardiac myocytes (RCMs) after ischemic–reperfusion (I/R) injury and supernatant from oxygen–glucose deprivation (OGD)–exposed primary rat neuronal cells (PRNCs). Cell viability of RCMs as revealed by calcein assay was down-regulated at 24 hours after I/R injury and treatment with supernatant harvested from PRNCs exposed to OGD compared with the addition of supernatant from non–OGD-exposed PRNCs. Similarly, mitochondrial activity using the 3-(4, 5-dimethyl-2-thiazoyl)-2, 5-diphenyltetrazolium bromide (MTT) assay revealed that the relative mitochondrial reductase activity of RCMs was significantly reduced at 48 hours after I/R injury and treatment with supernatant harvested from PRNCs exposed to OGD compared with the addition of supernatant from non–OGD-exposed PRNCs. Interestingly, both calcein and MTT assays revealed that I/R injury alone without the supernatant from the OGD-exposed PRNCs (DMEM treatment group represents the mean values over 48 hours) did not cause cardiac myocyte death.

positive. Moreover, RCMs cultured with the supernatant from OGD-exposed PRNCs showed significant time-dependent increase of positive cells against all cell death markers compared with the control. Consistent RCM alteration was recognized in all cell death markers by 24 hours after I/R injury. Of note, MAP1LC3A positivity was the most sensitive cell death marker altered in RCMs which was significantly increased even in the early phase (2 and 6 hours) after I/R injury, suggesting that the ischemic stroke robustly affected the autophagic pathway over the apoptotic and necrotic cell death mechanisms, in rendering toxic effects on the heart.

RCM viability as revealed by calcein assay supported the immunocytochemical results. By 24 hours of reperfusion, the treatment groups exhibited significantly lower viability than the other groups. In the mitochondrial activity assay, the group exposed to 48 hours of reperfusion exhibited the lowest viability compared with all groups.

In vivo results revealed all cell death markers were detectable in both the brain and heart. Interestingly, Caspase 3 (apoptosis marker) and MAP1LC3A (autophagy marker) are positive in contralateral side of brain, suggesting that the ischemic cell death in the ipsilateral side of brain (damaged brain area) may spread to the contralateral side of brain (intact area).

The converging results between the present in vitro and in vivo studies support the notion of an indirect pathological pathway of cell death originating from the brain to the heart. In particular, that the supernatant from the PRNCs after OGD produced toxic effects on RCMs suggests that soluble factors secreted by the ischemic brain cells may convey cell death signals to cardiac myocytes. It is likely that extractions of tissues (albeit, soluble factors) from stroke brain may render toxicity to the heart. The cell death cascade associated with ischemic stroke regulating the cardiac cell death suggests that the damaged or dead neuronal cells likely started to secrete soluble toxic factors at the early stage of ischemic insult, then the soluble factors subsequently reached the heart via the circulatory system at the later stage of ischemic injury. The present study thus offers a complementary indirect pathological link between ischemic stroke and cardiac failure, adding to the reported direct insular cortex regulation of heart rhythms.[7,31]

The toxic molecule's identify secreted by the ischemic brain remains to be determined, and subsequently, the specific mechanism is still unknown. With soluble toxic factors, adverse effects to the other vital organs in addition to the heart may be recognized and warrant further investigations. The routine clinical procedure is to check for any brain dysfunction following heart compromise. The present study suggests that a closer examination of heart function should be considered as part of the diagnosis following ischemic stroke.

The present study examined the effects of ischemic stroke on heart alterations, which parallels a series of studies demonstrating that cardiac arrest may lead to or accompany ischemic stroke.[19,20,32,33] Altogether, these 2 lines of investigations implicate an overlapping cell death signaling pathway between ischemic stroke and cardiac arrest. The understanding of the molecular, cellular, and anatomic changes that occur in stroke and cardiac failure may reveal novel treatment strategies that will aid the clinical outcomes of patients suffering from these 2 maladies.